Journal of Hydrology 598 (2021) 126208

Contents lists available at ScienceDirect

Journal of Hydrology

journal homepage: www.elsevier.com/locate/jhydrol

Research papers

Modeling lake outburst and downstream hazard assessment of the Lower Barun Glacial Lake, Nepal Himalaya

Ashim Sattar [a], Umesh K. Haritashya [a,*], Jeffrey S. Kargel [b], Gregory J. Leonard [c], Dan H. Shugar [d], Donald V. Chase [e]

[a] Department of Geology and Environmental Geosciences, University of Dayton, Dayton, OH 45469, USA
[b] Planetary Science Institute, Tucson, AZ 85719, USA
[c] Lunar & Planetary Laboratory, Department of Planetary Sciences, University of Arizona, Tucson, AZ 85721, USA
[d] Water, Sediment, Hazards, and Earth-surface Dynamics (waterSHED) Lab, Department of Geoscience, University of Calgary, Alberta T2N 1N4, Canada
[e] Department of Civil and Environmental Engineering and Engineering Mechanics, University of Dayton, Dayton, OH 45469, USA

ARTICLE INFO

This manuscript was handled by Marco Borga, Editor-in-Chief, with the assistance of Marco Toffolon, Associate Editor

Keywords:
Glacial lake
GLOF hazard
Himalaya
HEC-RAS

ABSTRACT

Climate change-driven retreat of glaciers is producing thousands of glacial lakes across mountain regions. These lakes generally grow, coalesce into larger lakes that may produce increased downstream hazards and risks due to glacial lake outburst floods (GLOFs). This study assesses such hazards of Lower Barun Lake located near Mount Everest, Nepal. We model a series of scenarios, including two potential avalanches that enter the lake from the surrounding slope and eight potential GLOFs from the lake. To evaluate the susceptibility of the frontal moraine to overtopping, we characterize the initial avalanche-induced surge of water over the moraine caused by the kinetic energy of arriving masses and possible tsunami-like events. Further, we present physical hydrodynamic models that reveal the hazard from the potential overtopping and GLOF events along the Barun-Arun river valley. Special attention is given to analyze the flow hydraulics at six downstream settlements. To estimate potential impacts at each location, two extreme-magnitude, two high-magnitude, two moderate-magnitude, and two low-magnitude GLOFs were hydraulically evaluated for the present lake dimension and the modeled future growth of the lake. As with most hydrological processes, the magnitude and frequency of GLOFs from Lower Barun Lake have an inverse, albeit uncertain, relationship, but the potential impacts on people and infrastructure are extremely sensitive to the events' magnitude. The flow dynamics results indicate that an overtopping flood without erosion of the damming moraine causes minimal impact in the valley. The extreme-magnitude and high-magnitude GLOF cases, where the moraine is incised, have a larger impact but differ greatly in magnitude at each of the downstream settlements. The moderate-magnitude and low-magnitude GLOFs, while the most frequent type, have limited volume and peak discharge, causing less impact downstream. Our calculations only portray the part of the hydrograph representing lake overfill due to a volume of ice or rock entering the lake, and the volume of the lake that could drain from a breach of the damming moraine down to specified depths over specified time periods.

1. Introduction

Rising global temperatures have increased glacier melting during this century at rates more rapid than in the previous century (Bolch et al., 2012; Kraaijenbrink et al., 2017; Roe et al., 2017). As meltwater becomes more voluminous, runoff can accumulate in depressions on thinning and sagging glacier surfaces, or in front of receding glaciers, and form moraine-dammed lakes such as Lower Barun in Nepal (Linsbauer et al., 2016; Haeberli et al., 2016; Sattar et al., 2019b). Moraine-dammed glacial lakes are the most common sources of glacial lake outburst floods (GLOFs) (Watanbe and Rothacher, 1996; Westoby et al., 2014). GLOFs have been observed many times since the end of the Little Ice Age (Vuichard and Zimmermann, 1987; Kargel et al., 2011; Carey et al., 2012; Clague and O'Connor, 2015; Vilímek et al., 2015; Anacona et al., 2015a; Paul and Bolch, 2019). However, GLOFs emanating from moraine-dammed lakes worldwide became far more common in the 1930s, an increase believed to be due to lagging responses to the end of the Little Ice Age. Since then, the incidence of GLOFs has fluctuated, first

* Corresponding author.
E-mail address: uharitashya1@udayton.edu (U.K. Haritashya).

https://doi.org/10.1016/j.jhydrol.2021.126208
Received 21 September 2020; Received in revised form 25 January 2021; Accepted 10 March 2021
Available online 16 March 2021

rising sharply and then falling somewhat since the 1980s (Harrison et al., 2018); yet it is expected to increase within parts of the Himalaya in the coming decades (Veh et al., 2020).

Moraine-dammed lakes are confined by end moraines or lateral moraines, with ice forming the up-valley lake margin until the glacier retreats farther and detaches. These moraines, however, usually consist of unconsolidated sediment, thereby making dam structures unstable compared with bedrock dams. Many of the moraines, especially in the Himalaya, initially contain ice (Richardson and Reynolds; 2000), which provides greater structural strength but eventually melts, leaving unconsolidated sediment and poor structural support to the dam. As the dams degrade due to erosion or melting of the ice, the lakes may gradually lower or become infilled with sediment, and slowly disappear. Sudden GLOFs from moraine-dammed or any other types of naturally dammed glacial lakes (supraglacial or ice-marginal) sometimes occur and pose risks to downstream infrastructure and communities (Osti and Egashira, 2009; Kropáček et al., 2015; Allen et al., 2016). As lakes continue to grow in number and size globally (Shugar et al. 2020), so does the cause for concern. GLOFs from moraine-dammed lakes may be triggered by (1) overtopping and erosion of the moraine dam caused by waves generated from ice avalanches, rockfalls, or calving; (2) meteorological conditions, especially extreme rain events, which may partly melt ice in the moraine dam and weaken the moraine, or cause overfill and thermal and physical erosion of the moraine, or induce a mass movement into the lake; (3) degradation from within the moraine dam (melt-through due to seepage from the lake and physical erosion—piping; or flotation of the moraine's buried ice by the hydrostatic gradient imposed by the lake); (4) a small GLOF, perhaps from a supraglacial pond, may overfill a moraine-dammed lake; or (5) seismic activity, when strong ground motion destabilizes the damming structure (Richardson and Reynolds, 2000; Westoby et al., 2014). These potential triggers each involves a stochastic chain reaction sequence, which cannot be explicitly predicted but may be understood either statistically for a population of similar lakes or individually through scenario modeling. Here, because we are investigating one lake, we take the latter approach.

All trigger mechanisms associated with GLOFs can range in magnitude and severity, depending on the lake's and terrain's individual details, including: (1) the lake's total drainable volume; (2) the internal sedimentological structure of the moraine dam, which can have low internal friction and high propensity to break up suddenly and cause high, peaked outbursts; or alternatively can have high internal friction and produce robust boulder armoring of drainage conduits and thus limit erosion and reduce peak discharge; (3) the amount, distribution, and structure of buried ice in the end moraine, which can control the likelihood and rate of melt-through piping, and can cause large changes in the moraine's structural integrity; (4) the width-to-height ratio of the moraine dam, for instance, a dam that is sharply peaked can readily and quickly break up, whereas a broad dam is more robust; (5) the height of the moraine dam, both the freeboard, which controls the damage and amount of overtopping for a given size of the wave, and the down-valley slope that partly controls the hydraulic pressure; (6) the lake's position with respect to its surrounding topography, which can either allow large mass movements to enter the lake rapidly and with large and sudden kinetic energy input, or not; (7) the mass of unstable hanging glaciers/snow or perched, fractured bedrock on adjacent mountain slopes; or (8) the lake bed and shore structure that can either cause tsunami waves to ramp up sharply, or undergo constructive wave interferences, or cause tsunami waves to diffuse harmlessly.

We note that one recent example of a mass movement-induced displacement wave caused overtopping of a moraine dam having 80 m of freeboard, so these waves can be rather extreme (Hubbard et al., 2005; Emmer, 2017). More modest impulse wave overtopping by about 5 m, caused, for example, by a large ice avalanche into Lake 513 in Peru (Worni et al., 2014), and similar to the smallest avalanche-triggered events modeled in this paper, can nonetheless generate damaging debris flows.

The rapid growth in the size and number of glacial lakes, along with rapid increases in infrastructure development (e.g., hydropower plants, roads, and bridges) and population in mountainous regions have catalyzed the need for: comprehensive regional and global mapping of glacial lakes (e.g., Campbell and Pradesh, 2005; Bajracharya and Shrestha, 2011; Emmer et al., 2016; Shukla et al., 2018; Shugar et al., 2020), comparative hazard and risk assessment (Thakur et al., 2016; Sattar et al., 2019a; Maskey et al., 2020), GLOF reconstruction (Majeed et al., 2020), prioritization for mitigation efforts (Khanal et al., 2015), assessment of earthquake aggravation of GLOF hazards (Kargel et al., 2016), detailed field, remote sensing, and modeling evaluation for GLOF hazard mitigation (Somos-Valenzuela et al., 2015; Kargel et al., 2016), and implementation of mitigation designs and consideration of coupled mitigation and economic development opportunities at glacial lakes (Regmi et al, 2017; Emmer, 2018).

In disaster risk assessment and management, risk conventionally involves the confluence of hazard, vulnerability, and exposure (e.g., Lavell et al., 2012); or if these are quantified, then the risk is the product of these components. The relative risk a GLOF may present to the downstream region depends on the hazard components consisting of peak discharge and cumulative discharge, which are functions of the drainable volume of the lake, condition of the damming moraine, potential GLOF triggers (listed above), and overtopping due to external impact which together determines the hazard; and the exposure and vulnerability of elements downstream of the lake (infrastructure, human life, and ecological values, including the resilience of these at-risk components). The risk that a potentially dangerous lake may present to the low-lying areas may be unrecognized unless a detailed hazard and risk assessment are undertaken. GLOF hazard assessments often contain inherent uncertainties as outburst events are hypothesized to occur in the future due to a variety of potential triggering processes. However, applying variable assumptions and conditions within hydrodynamic modeling, based on the spatial and geological characteristics of a lake and its surroundings, allows us to understand how a valley will behave in a lake failure event. Furthermore, developing detailed assessments and models addressing extreme-magnitude scenarios are needed for responsive disaster preparedness and mitigation.

The purpose of this study is to evaluate the GLOF hazard associated with Lower Barun Lake, located in the Nepal Himalaya, by performing a series of modeling and downstream flood routing. Given the complexity of the possible GLOF triggers in the mountainous basin, our first objective includes identifying and modeling potential avalanche around the lake to evaluate the susceptibility of the damming moraine to overtopping and downstream propagation of the overtopping flow. Although we do not model the erosion of the frontal moraine, some points about this erosion are considered in Supplementary section-1. The second objective is focused on GLOF hazard assessment by assuming that an overtopping wave can initiate erosion irrespective of the trigger and lead to complete breaching of the moraine. Thus this objective can be broadly categorized into two parts (i) potential GLOFs originating from Lower Barun Lake at its current state (present lake), under the following scenarios: extreme-magnitude, high-magnitude, moderate-magnitude, and low-magnitude GLOFs (ii) consider the same scenarios for the maximum future extent and estimated volume of the lake. The latter builds on the first but considers the future volume and extent of the lake for all four scenarios. The magnitude in each scenario relates to modeled flood volume, which integrates the breach parameters, as flood volume tracks with both breach values on Table 1. To achieve the first objective, we used remotely sensed data, field-collected information of potential avalanches that could trigger a GLOF, and two-dimensional dynamic physical models, including RAMMS (Rapid Mass Movement Simulation) and HEC-RAS. For the second objective, we used remotely sensed data, field-collected lake bathymetry (Haritashya et al., 2018) and HEC-RAS hydrodynamic modeling. We do not consider the instances of cascading hazards (e.g., Kirschbaum et al. 2019), such as GLOF spilling from nearby Upper Barun Lake into Lower Barun Lake,

Table 1
Summary of the different GLOF scenarios. Future GLOF is based on a future lake extent.

Scenarios	GLOF Description	*PFV/Vw* ($*10^6 m^3$)	h_b (m)	T_f (h)	B_w (m)
1	Extreme-magnitude present-lake	101.2	104	0.6	222.1
2	High-magnitude present-lake	78.8	64	0.9	187.1
3	Moderate-magnitude present-lake	46.5	32	1.3	138.5
4	Low-magnitude present-lake	16.0	16	1.4	86.4
5	Extreme-magnitude future-lake	179.0	104	0.9	266.8
6	High-magnitude future-lake	139.5	66	1.2	225.9
7	Moderate-magnitude future-lake	82.8	33	1.7	167.6
8	Low-magnitude future-lake	26.9	16.5	1.8	102.5

because our focus is on the direct inputs of solid mass into Lower Barun Lake and downstream GLOF hazard assessment. The series of outburst flood events modeled in this study are used to evaluate the downstream impact of the different magnitude of floods originating from the lake in the present and the future, irrespective of the trigger mechanism.

2. Study area background and importance

GLOF studies in the Hindu Kush-Karakoram-Himalaya (HKKH) previously ranged from regional-scale assessments (Quincey et al., 2007; Worni et al., 2013; Nie et al., 2017; Veh et al., 2018) to site-specific hazard assessments (Osti and Egashira, 2009; Bajracharya and Mool, 2009; Fujita et al., 2009; Shrestha et al., 2010; Sattar et al., 2019a, 2019c). In the Nepal Himalaya, glacial lake studies include comprehensive glacial lake inventories (Reynolds and Taylor, 2004; Bajracharya and Mool, 2009; Khadka et al., 2018), identification of hazardous glacial lakes (Rounce et al., 2017), GLOF return period (Cook et al., 2018), and GLOF reconstruction (Byers et al., 2018). Among the largest glacial lakes in Nepal, Imja Lake (Imja Tsho) has been the most widely studied, including detailed GLOF modeling (Somos-Valenzuela et al., 2015; Lala et al., 2018), field-based geophysical investigation of the frontal moraine (Dahal et al., 2018), investigations of its evolution over the past few decades (e.g., Fujita et al., 2009; Haritashya et al., 2018), and flood risk and management (Cuellar and McKinney, 2017).

In the last two decades, however, nearby Lower Barun glacial lake (27° 47′ 51″ N, 87° 05′ 26″ E) in the Makalu region of Nepal has been

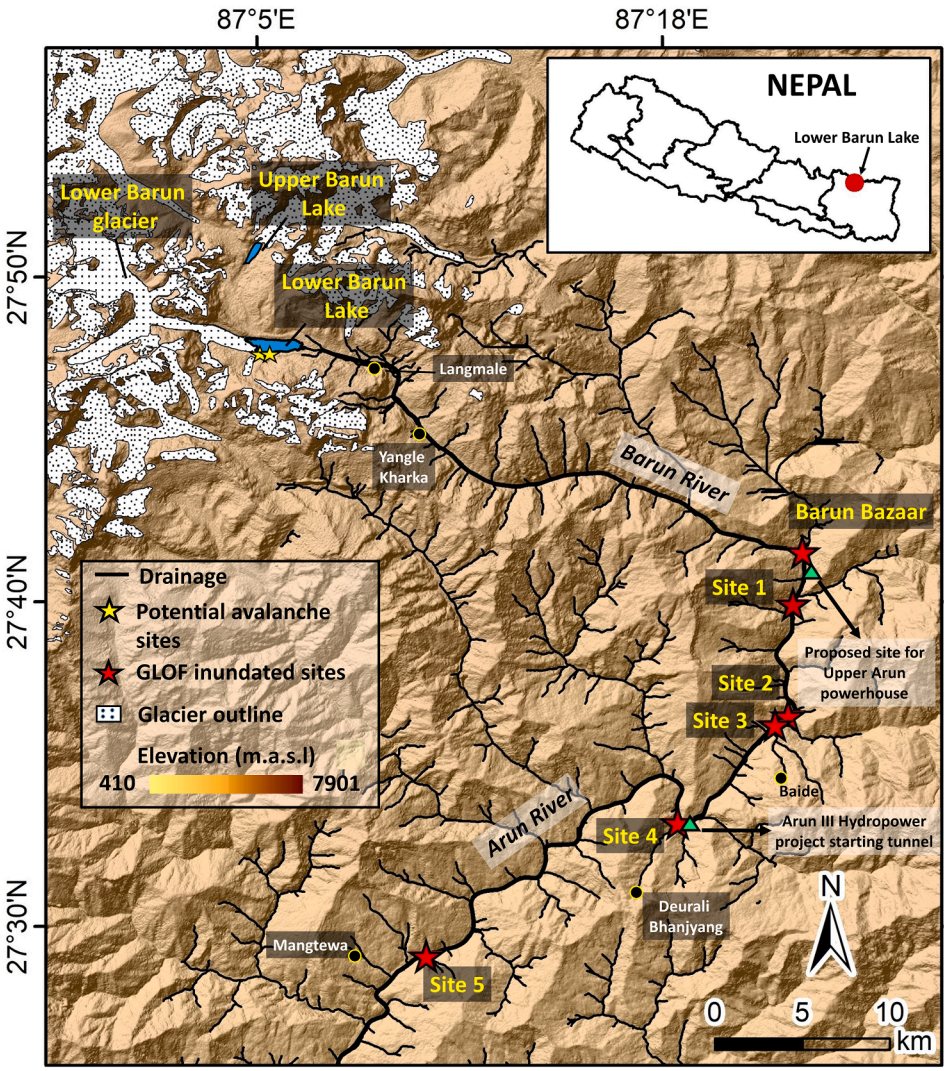

Fig. 1. Overview of the study area showing Lower Barun Glacier and Lower Barun Lake located in the Barun Khola basin, Nepal. The settlements (red stars) and hydropower sites (cyan triangles) are marked along the flow channel. The distances of the selected sites from the lake are 29.7 km (Barun Bazaar), 32.4 km (Site-1), 38.9 km (Site-2), 40 km (Site-3), 49 km (Site-4), and 70 km (Site-5).

growing rapidly, nearly doubling in area since the 1960s (to 2.2 km^2 in 2019) (Fig. S4). The lake is oriented east–west within the upper Barun drainage basin (Fig. 1) and it sits at an elevation of about 4550 m. The Barun River — a tributary of the Arun River (Sankhuwasabha District, Eastern Nepal) — drains from Lower Barun Lake and Barun Glacier, which feeds the lake. The Barun River also derives flow from Upper Barun Lake (and other smaller lakes in the basin), which drains down alongside Lower Barun Lake but is separated by a lateral moraine. As Upper Barun Lake itself poses a significant GLOF hazard, small future changes in drainage could produce a formidable cascading hazard situation. For now we only evaluate Lower Barun's hazard without involvement of Upper Barun Lake.

Lower Barun Glacier is characterized by numerous supraglacial lakes, ice cliffs, and thick debris cover in the lower ablation zone (Fig. 2 a-b). Lower Barun Lake is dammed by an ice-cored moraine (Dahal et al., 2018; Haritashya et al., 2018) on the east and the Barun glacier's terminus to the west. The damming moraine has a set of ponds through which the lake drains into and feeds the Barun River. In this regard, it is similar to Nepal's Imja Lake, and unlike Thulagi and Rolpa lakes, both of which drain directly over narrow end moraines without intervening ponds. Direct drainage over narrow, steep end moraines makes Thulagi and Rolpa lakes more hazardous or more likely to drain in a shorter period of time than Lower Barun and Imja lakes. However, of all these lakes, Lower Barun is by far the deepest known lake with the largest drainable volume, is the fastest-growing, and has the most rapid acceleration of growth (Haritashya et al., 2018; see Fig. S4); and the adjacent

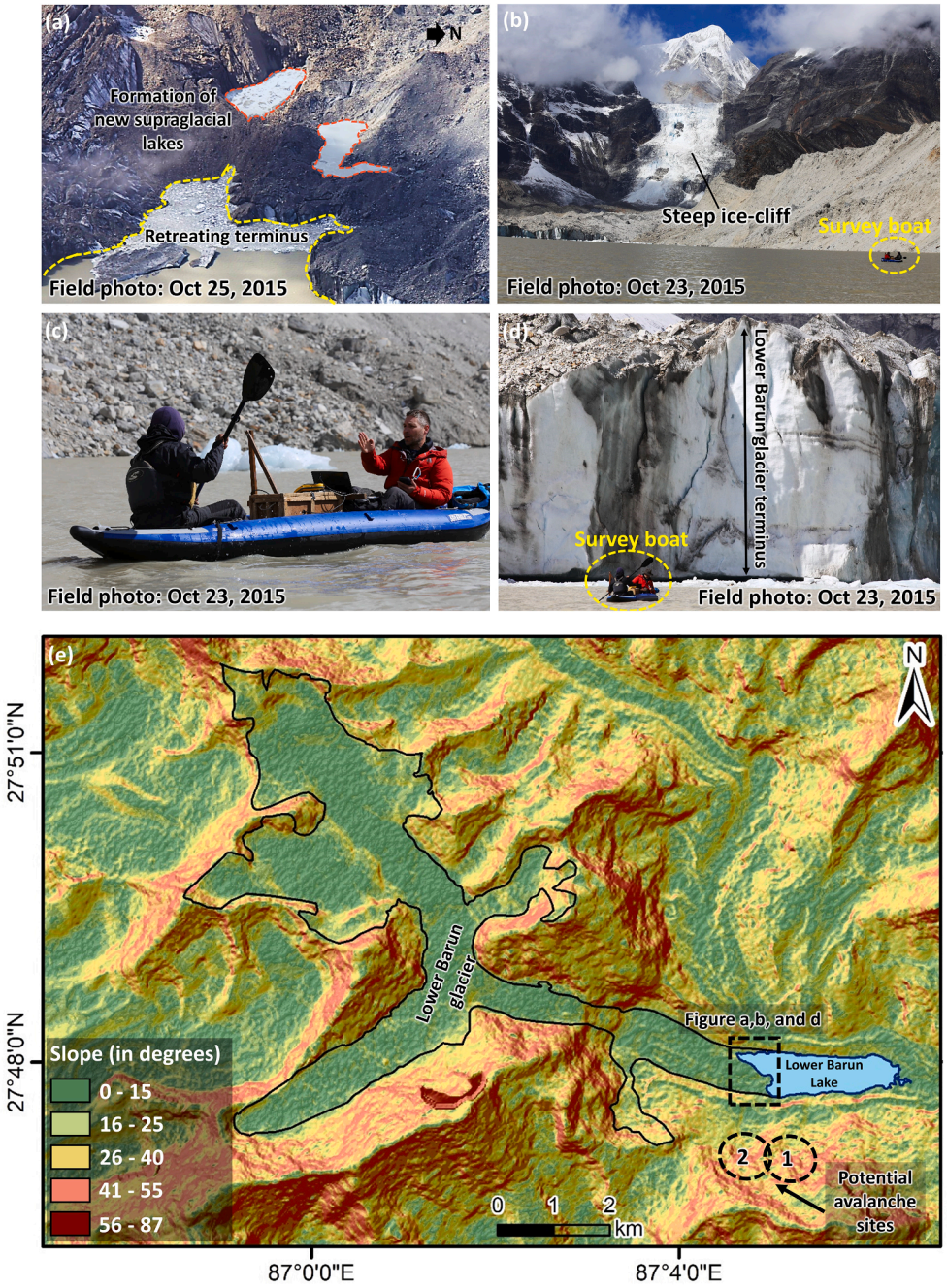

Fig. 2. (a) Field evidence of the retreating and thinning glacier terminus; (b) steep ice cliff upstream of the present glacier terminus; (c) bathymetric survey on a kayak mounted with SyQwest Hydrobox Sonar sensor; (d) Lower Barun glacier terminus.; (e) the Lower Barun glacier and lake showing the high and steep slopes (45-55 degrees) at locations of potential avalanches that could enter the lake.

mountain relief is immense. Furthermore, Lower Barun's end moraine is undergoing thermokarstic evolution, as is Imja Lake's, such that one of two things will happen: either the melting of ice within the end moraine will gradually lower the lake, or else the end moraine will evolve to a structure like that of Rolpa and Thulagi lakes, with a precarious, narrow end moraine dam. While the final state of Lower Barun's end moraine cannot be predicted with certainty, the hazard associated with moraine failure is increased if the moraine evolves into a narrow structure. Hazards are reduced if interior moraine-ice melts and lake levels fall.

The Barun valley has witnessed at least two known GLOF events (Meon and Schwarz, 1993; USAID, 2014; Byers et al., 2018). The first event flooded the Arun River in 1964 and was witnessed by the local people, but no other information about the source of the flood exists (Yamada and Sharma, 1993). The second outburst event occurred on April 17, 2017, and involved a rockfall and avalanche into Langmale glacial lake, located ~3 km east of Lower Barun Lake (Byers et al., 2018). The resulting flood deposited a huge volume of debris along the Barun River flow channel and impacted the settlements of Langmale and Yangla Kharke (6.5 km downstream, Fig. 1), containing Buddhist gompas and a few teahouses. This event blocked the confluence of Arun and the Barun rivers (29 km downstream from Lower Barun lake) and formed a short-lived landslide dammed lake. Yamada and Sharma (1993) identified Lower Barun Lake as potentially dangerous based upon the examination of aerial photographs. However, Kattelmann (2003) deemed Lower Barun Lake to be less threatening than other lakes in the broader region, such as Imja Lake, primarily due to the sparsely populated downstream regions. In any case, Lower Barun Lake has grown considerably since 2003 (Haritashya et al., 2018) exposing it to large mountain sides, and the Langmale event indicate that some rock units and mountain peaks in the valley exhibit large masses of unstable rock (Byers et al., 2018), posing a far greater threat than nearly two decades ago.

Of particular concern today are potential impacts of outburst floods on existing and proposed regional hydroelectric projects downstream of Lower Barun Lake. For example, the powerhouse of the proposed $1.4B, 1061 megawatt (MW) Upper Arun Hydroelectric project is located 2 km downstream from the confluence of Barun and Arun rivers (immediately above Site-1 in Fig. 1) (https://kathmandupost.com/money). Moreover, the 900 MW Arun III Hydropower project, also on the Arun River, has its starting tunnel located 49 km downstream of Lower Barun Lake (immediately west of Site-4 in Fig. 1). Both of these projects would be completely exposed to a GLOF from Lower Barun Lake. Therefore, it is important to investigate the range of potential GLOF hazards as a precursor to the kind of detailed physical field-science studies that preceded the engineered partial mitigation (lake lowering and stabilization of drainage outlet) of Imja Lake's GLOF hazard in 2014 (UNDP Imja Report, 2013; http://cfgorrp.dhm.gov.np/). Recently, several small settlements have formed along the lower Barun and Arun valleys (identified using multi-temporal high-resolution Google Earth imagery), and new hydropower projects could further spur growth in this valley, potentially exposing them to large GLOF risks in the future. Our study includes the potential impact of various GLOF scenarios on several downstream sites (Barun Bazaar and Site-1 to Site-5 as shown in Fig. 1). Apart from these settlements, numerous bridges and other small infrastructure exist along the channel downstream from Lower Barun Lake to Site-5.

3. Data

Bathymetric data were acquired during field investigation in October 2015 using an inflatable kayak-mounted SyQwest Hydrobox sonar echo-sounding sensor and modeled within ArcGIS using natural neighbor interpolation. More details about the methodology related to bathymetric observations, modeling, and uncertainty can be found in Haritashya et al. (2018). Lake bathymetric maps permitted an accurate simulation of the time-varying drawdown of Lower Barun Lake. Bathymetric information was also necessary to develop relatively accurate moraine breach models and determine the potential flood volume (PFV) released in different breach scenarios.

In avalanche simulations and hydrodynamic modeling, terrain properties such as surface elevation and surface roughness are often extracted using digital elevation model (DEM) and Landuse and Land Cover (LULC) composites, respectively. Here we used an Advanced Land Observing Satellite (ALOS) – Phased Array type L-band Synthetic Aperture Radar (PALSAR) DEM with a spatial resolution of 12.5 m. The ALOS PALSAR DEM is a radiometrically terrain-corrected elevation product released globally in October 2014 by the Alaska Satellite Facility (https://asf.alaska.edu/data-sets/derived-data-sets/alos-palsar-rtc/alos-palsar-radiometric-terrain-correction/). It has been successfully used for dynamic GLOF routing previously in the Himalaya (Dhote et al., 2019; Sattar et al., 2019a; Maskey et al., 2020). Most models either use a constant value of Manning's roughness coefficient or separate values for upstream and downstream routing. We used Landsat-8 derived LULC product (30 m) (Uddin et al., 2015) to extract pixel-based Manning's roughness coefficients along the flow channel. This enables us to define ground-channel friction in a spatially distributed pattern for accurate hydraulics.

For glacier bed mapping and future lake-volume estimation, we used the ALOS-PALSAR DEM, glacier outlines (RGI 6.0), and manually digitized glacier flowlines as inputs to generate an ice-thickness model (Linsbauer et al., 2012). We also employed the ensemble ice-thickness (Farinotti et al., 2019) and DEM for a comparative analysis of the glacier bed. Here, the glacier ice-thickness distribution (RGI160-15.03366) (Farinotti et al., 2019) was used to derive the glacier bed and the frontal overdeepening extent.

4. Methodology

The entire methodology of this study is summarized in Fig. 3, and details of each component are presented below.

4.1. Future lake extent and volume

To calculate the lake's future volume, we estimate the maximum extent of Lower Barun Lake by mapping the glacier bed using a spatially distributed glacier ice thickness product and DEM (Fig. 3 and Fig. 5a). Lacking ice thickness soundings and subglacial bed topography, we instead used the Glacier bed Topography (GlabTop) method (Linsbauer et al., 2012) and the ensembled ice thickness (Farinotti et al., 2019; see section 3 for data used) to calculate the glacier bed of Lower Barun Glacier. GlabTop is a shear-stress based model used to calculate ice thickness (h) for alpine glaciers, described by $h = \tau / (f \rho g \sin \alpha)$, where f is the shape factor, ρ is the ice density, g is the gravitational acceleration, and $\sin \alpha$ is the slope of the glacier. The ensembled ice-thickness is an average product derived using four different ice thickness models (Farinotti et al., 2019). We used three different shape-factors for glacier bed calculation using GlabTop ($f = 0.6$, 0.7, and 0.8). We also completed a raster-based calculation of ice thickness to derive the distributed glacier bed for all three values of f. An overdeepening site is extracted using raster-based operations in a GIS platform (ArcMap 10.7.1). By "overdeepened," we mean that the glacier bed extends to a lower elevation than the areas immediately downvalley from the lake.

The future lake extent and volume are obtained by interpolating between the current lake bathymetry (resampled to 25 m) and the modeled overdeepened bathymetry of the glacier-bed (e.g., Fig. 5b). We compare the four different modeled glacier-bed outputs (GlabTop-0.6, 0.7, 0.8, and ensemble output) with the glacial lake extent and field measured depths. The validated glacier bed is further used to calculate the volume of the frontal overdeepening site of the glacier. The future lake volume for our hazard assessment analysis is calculated by combining the current lake volume (from bathymetry data) and the volume of frontal overdeepening (both spatially resolved at 25 m). This

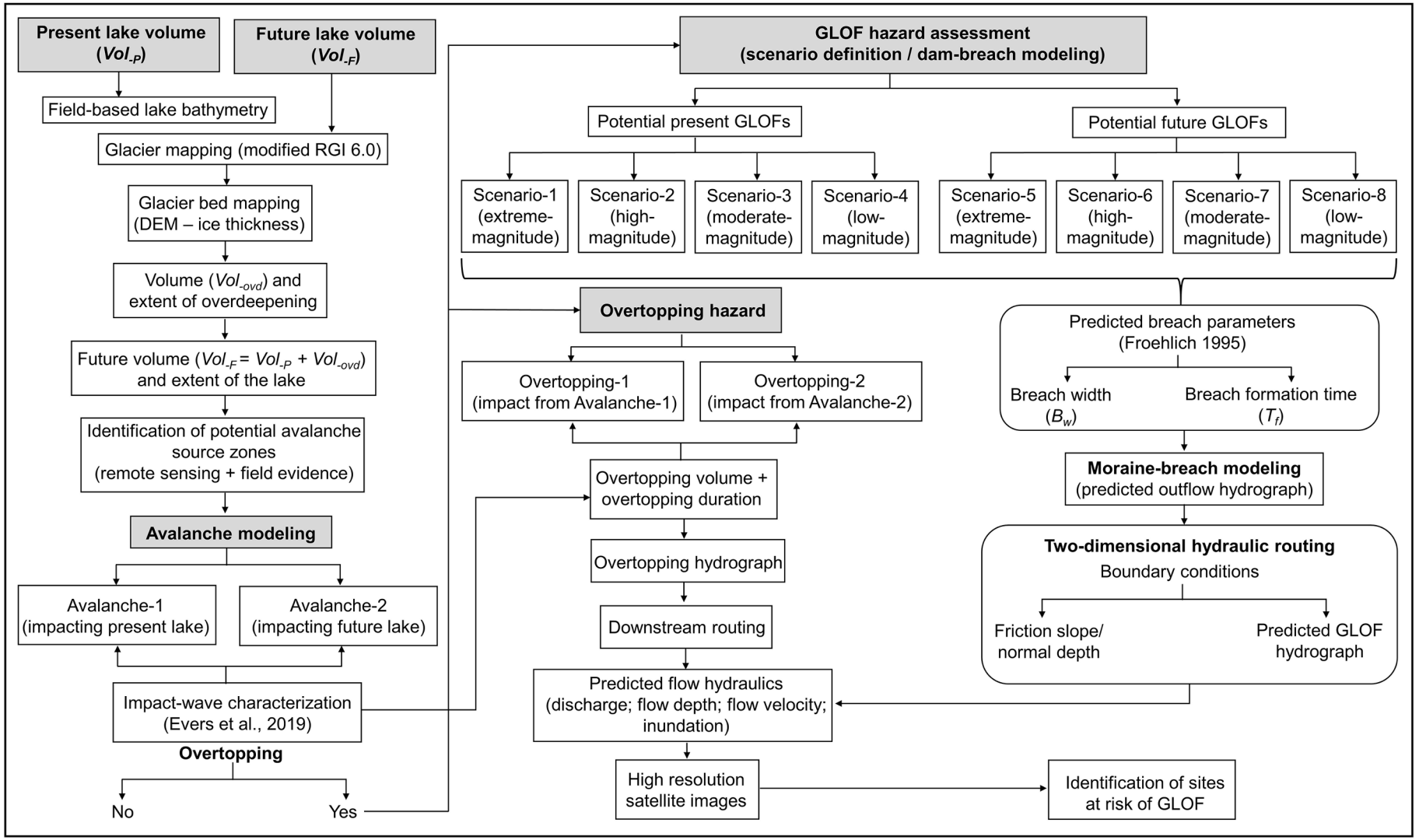

Fig. 3. The overall methodology adopted in the present study.

method to identify and map glacier bed overdeepening has been successfully used both at the global scale as well as locally in the Himalaya (Linsbauer et al., 2016; Frey et al., 2010; Haeberli and Linsbauer, 2013; Sattar et al., 2019b). The growth model also provides a good indication of how closely the west end of the lake will approach the high and steep adjacent mountain relief shown in Fig. 2e.

4.2. Potential GLOF triggers and overtopping

We identify two potential weak zones around the lake from where ice avalanches could trigger any of the GLOFs considered in this study (Fig. 2e); hence, we have modeled the avalanche impacts to determine if their impact waves overtop the frontal moraine. The avalanche locations were not picked arbitrarily but are based on our field observation (Fig. S5) and hazard assessment of Rounce et al. (2016) that identified slopes between 45° and 60° as being avalanche-prone, and where glacier ice masses appear to hang precariously. Most of these slopes host snow/ice perched atop a steep bed, which can be a potential trigger for any of the modeled GLOFs in this study. A significant avalanche emanated from one of these slopes during fieldwork, and a time-series of the avalanche has been captured (Fig. S5). The average speed of the avalanche as it crossed the lake was ~100 km h^{-1} (27.7 m s^{-1}), calculated from the time it took to cross the width of the lake. That is both measured and partly inferred by knowing approximately when it first reached the lake as the camera location and the route down the mountain is known, and the vectors from the camera to the lake shore can be closely estimated. The avalanche did not lead to the overtopping of the lake. Therefore, we model a higher magnitude potential-avalanche originating from the same location (Avalanche-1). For the second trigger (Avalanche-2) that can potentially have an impact on the future lake, we recognize another major slope with hanging snow/ice that occurs adjacent to the site described above, as a potential avalanche source zone. As discussed above and highlighted by Haritashya et al. (2018), the lake could grow up to this point towards its western end, rendering it vulnerable from large-scale avalanching from the surrounding slopes. Another important potential GLOF trigger is Upper Barun Lake, which could drain suddenly into Lower Barun Lake. However, that is a unique trigger mechanism that we are not evaluating in this paper.

The severity of these ice/snow mass movement triggering events has a relation to the volume of water displaced and the condition of the moraine. Thus, impulsive expulsion of water by the kinetic energy of a mass input is considered. We use RAMMS to model two potential avalanches. RAMMS is based on Voellmy-Salm finite volume method that solves the mass flow equations in two-dimension (Christen et al., 2010). The flow rheology of a mass movement is governed by the release area, volume, density of the material, friction parameters, and the underlying topography. Here, we define the release area for two potential avalanches by selecting the contiguous pixels with high slope angles (45°–60°). We define ice/snow thickness as 4.7 m and 4.9 m for Avalanche-1 and Avalanche-2, respectively, releasing a total volume of 11.2 × 10^5 m^3 of ice/snow (Rounce et al., 2016) in each case. The density (ρ) of flow material is considered as 1000 kg m^{-3} (ice with some rock debris and liquid water). Friction parameters include the Coulomb friction (μ) and turbulent friction (ξ) (Bartelt et al., 2013), which were set as 0.12 and 1000 m s^{-2} for μ and ξ, respectively. These input values are widely used to model avalanches in snow-covered and glaciated terrain (Schneider et al., 2014; Somos-Valenzuela et al., 2016; Frey et al., 2018). The outputs were obtained as avalanche runout distances (m), flow depths (m), and flow velocity (m s^{-1}).

The avalanche-induced impact waves generated by the potential avalanches were modeled empirically using the Evers et al. (2019) model. A previous approach of Heller and Hager (2010) has been used for avalanche-induced impulse-wave characterization in glacial lakes in the Himalaya (Lala et al., 2018; Byers et al., 2018, 2020). Based on the same principles as Heller and Hager (2010), the approach of Evers et al. (2019) computes the overtopping wave height, overtopping velocity, and volume due to impulse waves based on updated studies. The inputs to the model, such as impact velocity, impact volume, slide thickness, and slide width, are derived from the RAMMS outputs. We calculated the impact volume as the volume entering the lake at the end of an avalanche. The impact-wave run-up angle and freeboard were calculated using DEM and high-resolution Planet data. Based on the overtopping characteristics of the impact wave, the overtopping volume (in m^3) and duration (in sec) from Lower Barun Lake is determined for each impact (Avalanche-1 and Avalanche-2). Further, the overtopping hydrographs were calculated based on the total overtopping volume and duration were used as an input for downstream flood routing. We use HEC-RAS (v 5.0.7) (https://www.hec.usace.army.mil/software-/hec-ras/), a two-dimensional hydrodynamic model to evaluate the downstream propagation of the overtopping wave. The hydrodynamic module solves the depth-averaged two-dimensional shallow water equations (Saint-Venant Equations) in an unsteady flow. The time-series of flow depth (D_f) and flow velocity (V_f) obtained as output in a spatially distributed manner are used to evaluate the GLOF hydraulics downstream of the lake. The detailed model settings for 2D flood routing are given in the Supplementary section-2.

4.3. Present and future GLOF hazard assessment and scenario modeling

Since overtopping flows can induce dam erosion, forming an initial breach followed by progressive breach enlargement (Singh, 1996), we assume the same in the case of Lower Barun Lake. Therefore, overtopping modeling is followed by dam-breach flood (GLOF) modeling. Here we evaluate a series of potential GLOFs that can originate from Lower Barun Lake assuming moraine breaching of different magnitudes, potentially triggered by the overtopping wave, and some scenarios implying that a dam breaching erosion event has occurred. Whereas we include a plausible functional form of the developing breach (a sine function), the function we select is not an actual erosional model. Therefore, our GLOF modeling is based on the hypothetical magnitude of the water released (PFV) and the release duration, not the sedimentological erosion modeling associated with the overtopping.

We use HEC-RAS (v 5.0.7) one-dimensional and two-dimensional hydrodynamic model to study eight potential GLOF events based on the varied breach parameters that represent current lake conditions (scenarios 1–4) and maximum future lake extent (scenarios 5–8) while keeping moraine dam geometry, downstream valley geomorphology, and river hydrological conditions the same in every simulation. (Table 1; Fig. 4). HEC-RAS has been used successfully in one and two-dimensional hydrodynamic modeling of outburst floods in steep terrain like the Himalaya (Klimeš et al., 2014; Anacona et al., 2015b; Wang et al., 2018; Sattar et al., 2019a, 2019c, 2020). Our modeling assumes the continuation of the lake's rapid observed growth, but by including a wide range of potential GLOF scenarios, the effects of changing moraine-breach properties are indirectly included.

Each scenario has a unique set of parameters, including the height of the breach (h_b), time of moraine failure (T_f), breach width (B_w); all of which constrain the flood volume (V_w) released in a potential outburst event and are calculated using Froehlich (1995b):

$$B_w = 0.1803 K_o (V_w)^{0.32} (h_b)^{0.19} \quad (1)$$

$$T_f = 0.00254 (V_w)^{0.53} (h_b)^{-0.9} \quad (2)$$

The high accuracy and low prediction error of these sets of equations make it the most widely used empirical approach for modeling earthen-dam failures (Wahl, 2004). All the scenarios were modeled as a sine wave progression breach model where the initial breach forms slowly and speeds up with time as outflow velocities and shear stress increases through the breach. The output is obtained in the form of a breach hydrograph with a peak discharge (Q_{max}) for each modeled event considered for downstream routing along the flow channel. Each output

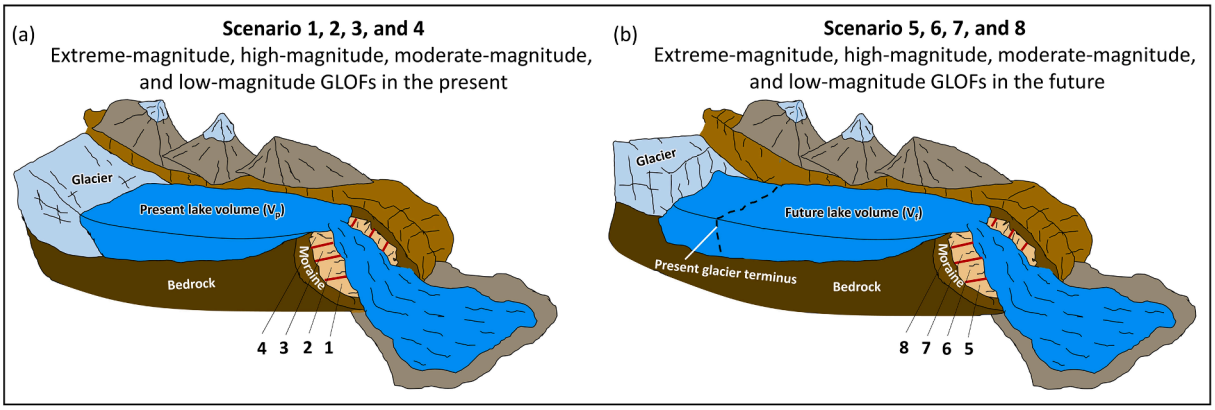

Fig. 4. Schematic showing the different dam breach scenarios of Lower Barun Lake, where Scenario-1 and Scenario-5 represent the potential extreme-magnitude events, Scenario-2 and Scenario-6 represent high-magnitude events, Scenario-3 and Scenario-7 are moderate-magnitude events, and Scenario-4 and Scenario-8 are low-magnitude events; the solid red lines show the respective breach heights. Note that the scenarios are modeled with or without any specific trigger.

hydrograph was evaluated by comparing it with empirically calculated peak outflow-discharge (Froehlich 1995a):

$$Q_p = 0.607 V_w^{0.295} h_w^{1.24} \quad (3)$$

here, we set up dam-break models for two extreme-magnitude events (scenario-1 and scenario-5), two high-magnitude events (scenario-2 and scenario-6), two moderate-magnitude events (scenario-3 and scenario-7), and two low-magnitude events (scenario-4 and scenario-8), all originating from Lower Barun Lake.

Our field investigation and analysis of remotely sensed data suggest that the frontal moraine has a hummocky surface signifying the presence of buried ice. Since no geophysical investigation of the frontal moraine is available, it is unclear how deep this buried ice is. Supplementary section-1 shows that in one sector, the debris cover is very thin, but it certainly is not thin everywhere. As a result and relying on our field knowledge of the lake's frontal moraine, the breach height in an extreme-magnitude case is considered till the point where the hummocky terrain ends, where the height appears to be 104 m. This moraine height is consistent with the findings of Reynolds and Richardson (2000) who found that the terminal moraines from the Neoglacial maxima often exceed 100 m in height where the resulting lakes can contain 1–20 million m^3 of water, presenting a serious hazard threat to the downstream regions. Furthermore, the more widely studied Thulagi lake, located in the Upper Marsyangdi catchment, northern Nepal, is dammed by a debris-covered stagnant ice body 100 m thick that dates back to the last glacial advance (Hanisch et al., 1998, 1999; Pant and Reynolds, 1999). Therefore, for modeling the extreme-magnitude GLOFs of Lower Barun Lake, it is assumed that breach incision occurs until it reaches the base of the moraine (i.e., h_b = 104 m; Table 1). Further, in the case of high-magnitude events, h_b is considered to be the mean depth of the lake (Fujita et al., 2013) and the corresponding V_w is calculated based on the lake bathymetry. In the moderate-magnitude scenarios, h_b is assumed to be half of the high-magnitude breach depths. And, in the low-magnitude GLOFs, h_b is half of the moderate-magnitude breach. The PFV from the lake in any of the above GLOFs depends on the bed topography (bathymetry) and breach dimensions of the frontal moraine. We calculate the drainable flood volume based on the height of the breach (h_b), as the present bed topography of Lower Barun Lake does not allow its entire volume to drain, even in an extreme-magnitude breach (i.e., volume below 104 m h_b does not drain) (Fig. 6a). The assumed floods are of water only and do not include ingested sediment in the total emitted flood volumes, the dynamical behavior of the flood (such as impulsive ejection of water from below h_b), or downstream deposited sediment. The hydraulic flood modeling also does not include bank erosional or depositional changes in channel/valley geometry during the events.

4.4. Dynamic routing and hydraulic assessment along the flow channel

Two-dimensional hydrodynamic routing of the breach hydrographs for each breach scenario (scenarios 1–8) was performed using HEC-RAS along the flow channel from Lower Barun Lake to Site-5, located 70 km downstream. The hydraulic behavior of the GLOF wave was analyzed at six different sites (Barun Bazaar, and Site-1 to Site-5; Fig. 1) along the flow channel based on flood discharge (Q), flow depths (D_f), and flow velocities (V_f). The Manning's roughness coefficient associated with the channel is extracted for the flow area using a Landsat-8 derived LULC (30 m) of Nepal (Uddin et al., 2015). Our pixel-based Manning's roughness distribution (n) for the given flow regime ranged from 0.035 to 0.17 based on the different LULC classes present along the flow area. Our approach using Landsat imagery can capture the large-scale roughness but not 1- to 30-m-scale roughness elements, so it is merely an approximation to what might be encountered by an outburst. It may apply strictly only to the largest modeled outburst events but could also apply to the smaller events if there is a scale-independent (fractal) roughness over the range of scales of the modeled floods. The detailed model settings are given in the Supplementary section-2. The model outputs were analyzed to evaluate the flow hydraulics of the GLOF wave along the channel. The result metrics are represented in the form of flood inundation limits (I_f) (km^2), discharge (Q) ($m^3\ s^{-1}$), flow velocity (V_f) (m s^{-1}), and depth (D_f) (m) at which the evacuated lake water travels down the Barun Valley.

5. Results

5.1. Future lake extent and volume

The Lower Barun future lake extent and volume were calculated using an ice-thickness approach where the present bathymetry of the lake was combined to the frontal overdeepening extent of the Lower Barun glacier. Of the four different outputs of modeled overdeepening (GlapTop $f = 0.6$, $f = 0.7$, $f = 0.8$, and ensembled output), the ensemble-model results (Farinotti et al., 2019) correlated most accurately to the present lake extent with a difference of <5% (Fig. S6). The ensembled ice thickness of Lower Barun Glacier has a maximum thickness of 258 m with surface elevation ranging between 4551 and 6669 m a.s.l. The depths of the frontal overdeepening range up to ~197 m (Fig. 5b). The spatially distributed bathymetry of the overdeepening site calculated using ice thickness and surface elevation data (Farinotti et al., 2019) occupies a total area of 1.62 km^2 extending approximately 2 km upstream from the present glacier terminus (Fig. 5b and Fig. 6b, c). The overdeepening zone terminates where the bed elevation abruptly rises into an ice cliff (Fig. 5c and Fig. 6b). The field-based lake bathymetry

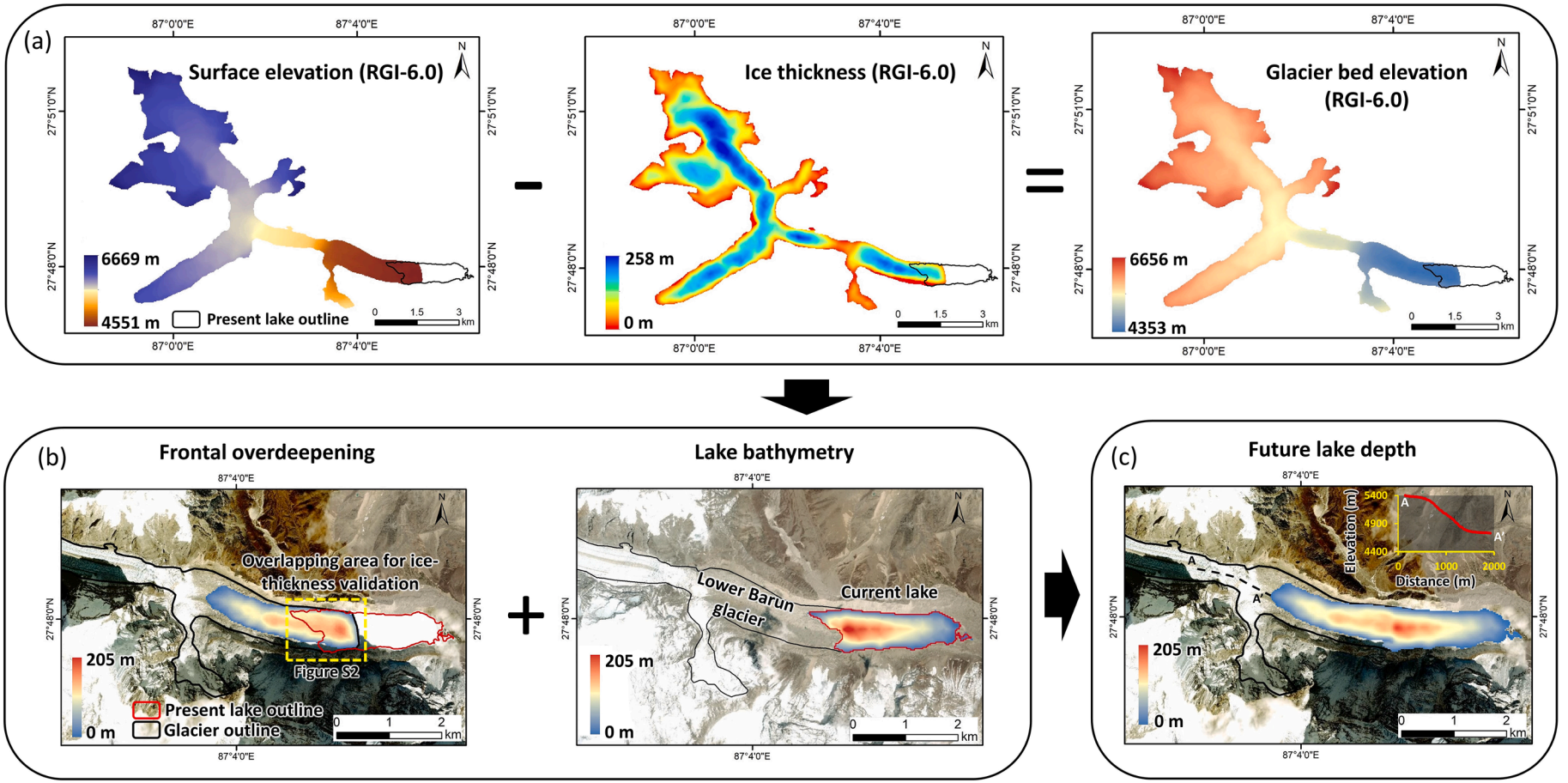

Fig. 5. Graphical representation of the raster-based operations for (a) mapping the glacier bed using spatially distributed ice thickness and DEM (Farinotti et al., 2019); (b) resampling and mosaicking depth distributions of the frontal overdeepening and the lake bathymetry to calculate (c) the future depth/volume of Lower Barun Lake.

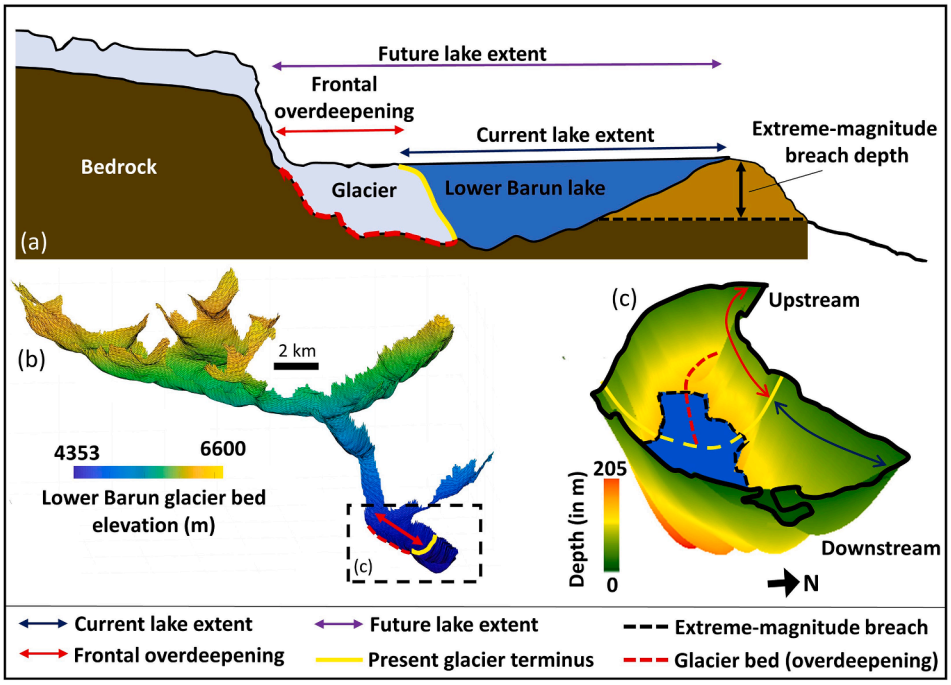

Fig. 6. (a) Cross-sectional profile of Lower Barun glacier and lake structure; (b) Glacier bed of the Lower Barun glacier; (c) 3-D (East-view) bathymetry of the future lake showing the frontal overdeepening, present lake extent, and the extreme-magnitude breach level.

reveals a maximum depth of 205 m with the deepest point located near the current terminus (Fig. 5b). The deepest point of the overdeepening (ensemble) occurs at about the same location as that of the lake bathymetry, i.e., if the ice were removed, the new lake bed would be about 197 m deep. The depth at the deepest point of the overdeepening (197 m) has a difference of $< 5\%$ compared to the bathymetric lake depth at that given point. The average difference in the depths (overdeepening bathymetry minus lake bathymetry) of the overlapping area (Fig. 5b and S6) is calculated to be less than 3%. The maximum depth of the future lake derived after combining the spatially distributed current lake bathymetry and overdeepening bathymetry is 205 m, which shows that the lake has already reached its deepest point. The future volume of Lower Barun Lake calculated by combining the bathymetries of the modeled frontal overdeepening zone plus the field-based lake bathymetry is 193.5×10^6 m^3, covering a total area of 2.69 km^2. This volume was used for future-lake GLOF hazard modeling, as discussed in the next section.

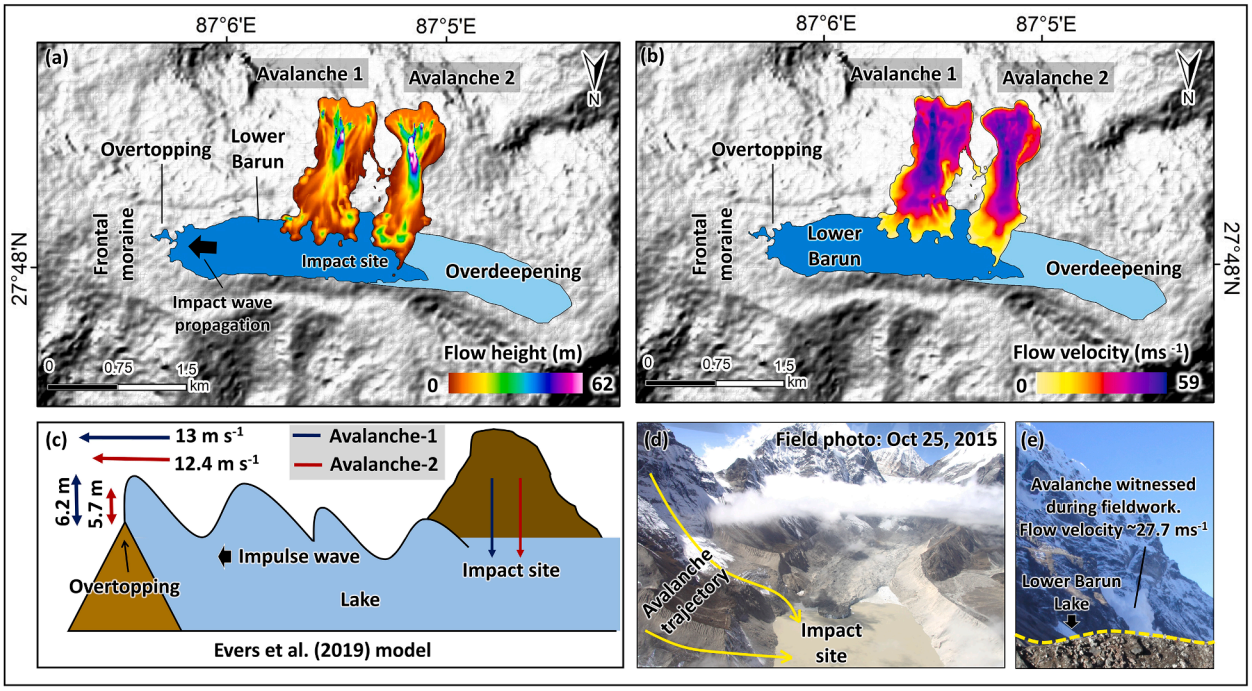

Fig. 7. (a) Flow depth (m), and (b) Flow velocity (m s^{-1}) of the two modeled potential avalanches; (c) modeled impulse waves and overtopping (Evers et al., 2019); (d) photograph showing the steep slope (avalanche source zone) located at the right surrounding slope, the modeled avalanche trajectory, and the impact site on the lake; (e) photograph of avalanche from the right slope witnessed during fieldwork.

5.2. Avalanche modeling and overtopping

We modeled two potential avalanches with their sources from the surrounding south slope of the lake, one of which has witnessed a previous avalanche recorded by the field team (Avalanche-1; Fig. S5 and Fig. 7e). In Avalanche-1, a total of 9.2×10^5 m^3 volume enters into the lake with a maximum velocity of 34 m s^{-1} (Fig. 7a and 7b). The maximum flow velocity is 59 m s^{-1} (212 km h^{-1}). The flow speed is double to that of the flow speeds of the avalanche witnessed during fieldwork. The modeled impulse wave generated at the site of impact approaches the frontal moraine at a speed of 13 m s^{-1} (Fig. 7c). The wave overtops the frontal moraine with a flow height of 6.2 m draining a total volume of 9.3×10^4 m^3. The second avalanche (Avalanche-2), with its source from another weak zone adjacent to the source of Avalanche-1, carries 9.1×10^5 m^3 of the total avalanche at a speed of 32.9 m s^{-1} to the lake. The resultant impulse wave overtops the frontal moraine with a flow height of 5.7 m and an overtopping velocity of 12.4 m s^{-1} (Fig. 7c) draining 8.4×10^4 m^3 of the lake volume. Although the model accounts for the water depth at the impact site, the calculation does not include the tsunami-type ramping up of wave amplitude and wave slow-down due to lake shallowing toward the moraine, but overall the modeling highlights the potential for large avalanches to generate powerful waves. It is clear from the avalanche simulations that the frontal moraine of Lower Barun Lake is susceptible to potential impact-waves that can lead to the overtopping and subsequent breaching, following which we evaluated the potential GLOFs of different magnitudes originating from the lake. We note that the higher magnitude events can also originate from these slopes and that the overtopping heights of our modeled waves are very small compared to some historic ones, such as that of a GLOF in Peru (Hubbard et al., 2005; Emmer, 2017). The overtopping hydrograph calculated for Avalanche-1 (impact-wave) has a peak of 9298 m^{3}s^{-1} with a total overtopping duration of 21 s (Fig. 8). For Avalanche-2 impact, the peak of 8300 m^{3}s^{-1} is calculated where the overtopping duration is 20 s. The overtopping hydrographs were routed downstream, revealing D_f reaching up to ~ 8 m and V_f reaching up to 25 ms^{-1}. Both the flood waves (Avalanche-1 and Avalanche-2) travel 18 km downstream of the lake, with overtopping from Avalanche-1being slightly of higher magnitude. The overtopping flood does not affect Barun Bazaar. At Yangle Kharke, D_f and V_f reaches up to 1.6 m and 1.4 ms^{-1}, respectively. These modeled events are thus likely to be a relatively high-frequency, low-magnitude type.

5.3. Moraine-breach and inter-comparison of GLOF discharge

GLOF hazard assessments of Lower Barun Lake were conducted based on eight potential moraine-breach events that vary dimensionally as a function of h_b, V_w, T_f, and B_w. The physics and dynamics of the breach's erosional process are not modeled. Each of the potential breach events produced a different outflow peak-discharge (Q_{max}) based on the given breach parameters (Fig. 9). In general, the future GLOFs resulted in higher discharges than the present-lake GLOFs due to increased lake water volume. Here we assume that breach depths can reach a maximum of 104 m in any (present and future) extreme-magnitude GLOF, if breach incision completely propagates down to the base of the moraine (Fig. 4 and Fig. 6a). Such events are rare in nature and depend on the moraine conditions and trigger magnitude. In the case of Lower Barun Lake, it potentially drains the volume in the water column above 104 m, i.e., the lake's maximum drainable flood volume. For example, the potential extreme-magnitude GLOF event (Scenario-1 present and scenario-5 future) produced a Q_{max} of 44,240 m^3 s^{-1} and 52,344 m^3 s^{-1}, respectively, immediately downstream of the lake (Fig. 9). A sharp rise is seen in the outflow hydrograph where Q_{max} is reached within 20 min after the initiation of the breach in both present and future cases, releasing a total flood volume of 101.29 $\times$ 10^6 m^3 and 179 $\times$ 10^6 m^3, respectively (Table 1). For other present scenarios (2–4), flood volume varies between 16 and 78.8 $\times$ 10^6 m^3 while Q_{max} is reached 28–64 min after the initiation of the breach in the present case. Similarly, for future scenarios (6–8), the peak is reached 26–58 min after the breach event initiation as it releases a flood volume of 26.9 to 139.5 $\times$ 10^6 m^3.

5.4. Hydraulic characterization of GLOFs along the flow channel

GLOF inundations were calculated for eight different dam breach scenarios with variations in their breach formation time (T_f), breach height (h_b), and breach width (B_w). We also evaluated Q (m^3 s^{-1}), V_f (m s^{-1}), and D_f (m) by flood routing of the individual breach hydrographs

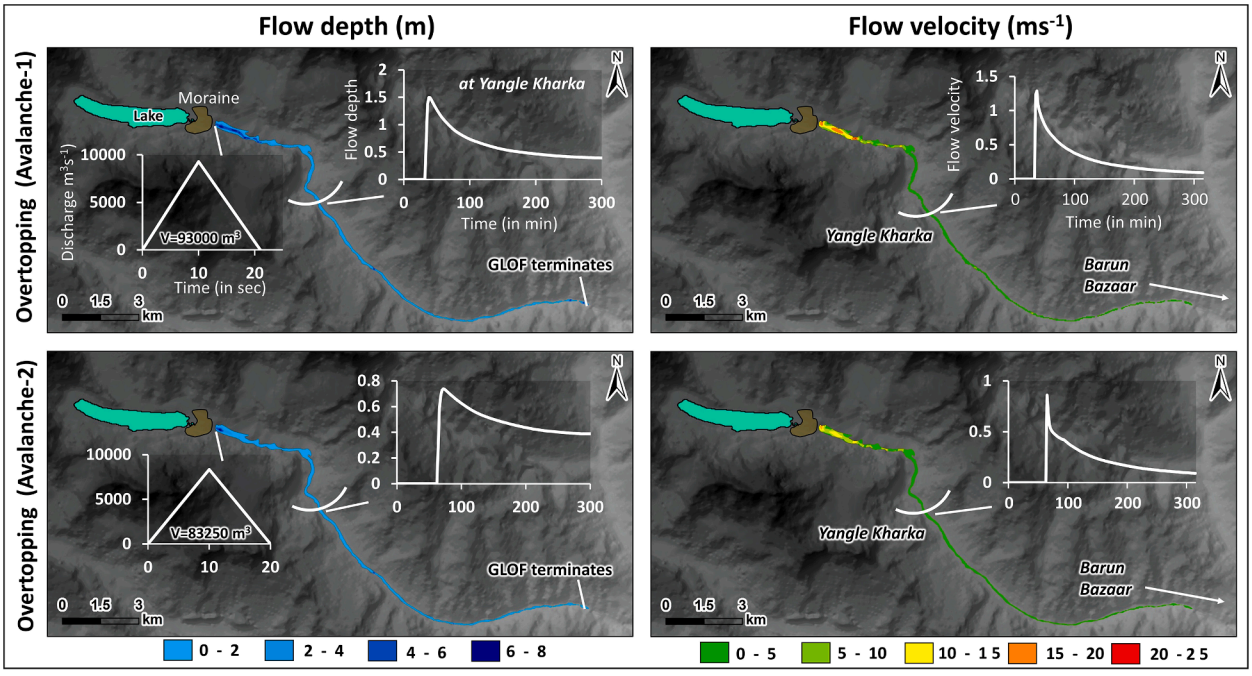

Fig. 8. Spatially distributed flow depths (D_f) flow velocities (V_f) in an overtopping flood resulting from the impact of Avalanche-1 (a,b) and Avalanche-2 (c,d) on Lower Barun Lake.

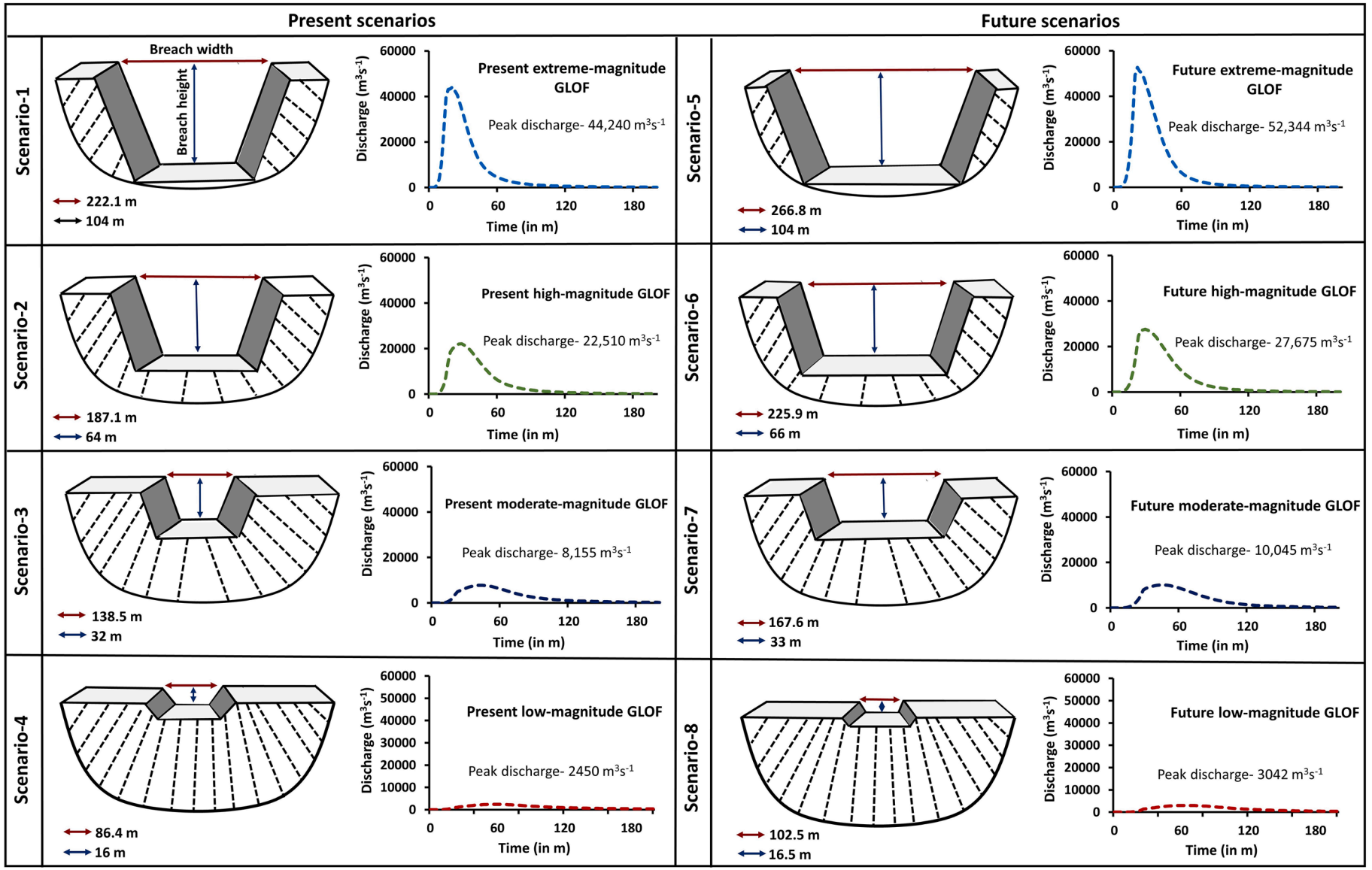

Fig. 9. Schematic showing the breach parameters (Froehlich, 1995b) for different GLOF scenarios and their corresponding outflow hydrographs; Scenario-1 and Scenario-5 represents the extreme-magnitude GLOFs, Scenario-2 and Scenario-6 represent the high-magnitude GLOFs, Scenario-3 and Scenario-7 represent the moderate-magnitude GLOFs, and Scenario- 4 and Scenario-8 represents the low-magnitude GLOFs of Lower Barun Lake.

obtained for each of the scenarios (Section 5.3; Fig. 9). This enabled us to characterize and compare the effects of flood-water progression from the various breach scenarios down the Barun and Arun Valley. Here we present the results of an inter-comparison of the flow hydraulics at six different sites downstream of the lake (Barun Bazaar, and Site-1 to Site-5; Fig. 1). Due to the large magnitude of the GLOF flows, any additional flow added by existing stream flows in the Barun and Arun rivers were considered negligible.

5.4.1. Inter-comparison of routed hydraulics of potential current-GLOFs

In Scenario-1 (present extreme-magnitude scenario), the GLOF wave first reaches Barun Bazaar 1 h 5 min after the initiation of the breach event. For scenarios (2–4), the arrival time at this site ranges between 1 h 12 min to 6 h 30 min. Here, D_f reaches up to 26 m with a maximum V_f of 9 m s^{-1} (Table 2; Figs. 10, 11, and 12). The GLOFs could potentially inundate a cluster of small houses located along the river-left bank of the Arun River (Fig. 13). The low-magnitude GLOF (Scenario-4) terminates before it reaches Site-2 and moderate-magnitude GLOF (Scenario-3) terminates before reaching Site-5.

At Site-1, the GLOFs potentially inundates a small settlement consisting of 10–15 houses and a bridge with D_f and V_f reaching up to 22 m and 6 m s^{-1}. Farther downstream, Site-2 and Site-3 (located ~1 km apart) reveal similar flow behavior, where D_f ranges from 20 m to 27 m and V_f between 1 m s^{-1} to 3 m s^{-1}. Here, three small settlements, one bridge, and 0.04 km^2 of agricultural land become inundated (Fig. 13). Among all the potential current GLOFs and the studied sites downstream (Site-1 to Site-5), including Barun Bazaar, a maximum D_f of 36 m (Scenario-1) is reached in Site-4, where the 900 MW Arun III Hydropower project has its starting tunnel. This is due to the sharp turn of the river channel towards the west. Here, the potential GLOFs have a major impact inundating a moderate-sized settlement, two bridges, and several roads (Fig. 13). As the potential GLOFs propagate downstream, they reach Site-5 (70 km downstream) with arrival timing of 4 h 48 min (Scenario-1) and 7 h 8 min (Scenario-2), where D_f reaches up to 19 m. Here, the GLOF wave has a maximum V_f of 3 m s^{-1}, though its flow energy attenuates as it propagates farther downstream.

5.4.2. Routed hydraulics of potential future-GLOFs

The hydrodynamic routing and flow assessments of the future GLOFs were evaluated for Scenarios 5, 6, 7, and 8 (Table 2). The routed hydrographs were calculated based on the lake's future extent and volume (193.5 × 10^6 m^3; see section 4.1). In a potential extreme-magnitude future GLOF event (Scenario-5), the drainable volume (V_w) from the lake is calculated to be 179.0 × 10^6 m^3 considering $h_b = 104$ m as a maximum breach depth (Table 1; Fig. 9). The flood wave arrives at Barun Bazaar a few minutes (~5 min) earlier relative to that of Scenario-1 (present extreme-magnitude GLOF). Here, the D_f and V_f reach up to 29 m and 11 m s^{-1}, respectively (Table 2; Fig. 12). This accounts for an increase of ~11 and ~20%, respectively, when compared to a present extreme-magnitude event. The at-risk infrastructure remains the same at Site-1, 2, and 3; however, the flow hydraulics are variable (Figs. 10–12). At Site-4, D_f reaches a maximum of 37 m with a peak V_f of 7 m s^{-1}. This is the highest velocity calculated at this site compared to all the other modeled GLOF events in this study. Here the inundation limits extend further southward, engulfing the maximum area containing infrastructure and settlements. The flood wave travels further down the valley for about ~3 km but has no impact due to the absence of infrastructure or settlement.

In Scenario-6, which represents a future high-magnitude GLOF, the flood wave encounters Barun Bazaar 1 h 22 min after the breach event (Table 2). Flow hydraulics indicate peak D_f and V_f are decreased by 4 m and 2 m s^{-1}, respectively, and its arrival time at Site-1 is delayed by 20 min compared to Scenario-5 (Fig. 12). At Site-2 and Site-3, the flow hydraulics show a reduction of D_f and V_f by an average of 9.5 m and 2 m s^{-1} at these sites compared to the extreme-magnitude future-lake GLOF. The flood wave arrives at Site-4 40 min later compared to an extreme-

Table 2
Flow hydraulics at different sites along the flow channel. The scenario that does not reach a specific site is given as "NR".

	Flood wave arrival (Time in h)							Maximum flow depth (D_f) (m)							Maximum flow velocity (V_f) (ms^{-1})							Discharge (Q) (m^3s^{-1})						
	SC-1	SC-2	SC-3	SC-4	SC-5	SC-6	SC-7	SC-8	SC-1	SC-2	SC-3	SC-4	SC-5	SC-6	SC-7	SC-8	SC-1	SC-2	SC-3	SC-4	SC-5	SC-6	SC-7	SC-8	SC-1	SC-2	SC-3	SC-4	SC-5	SC-6	SC-7	SC-8
Barun bazaar	1.07	1.43	2.33	6.5	1.01	1.37	2.07	3.0	26	22	11	2	29	24	13	9	9	9	5	3	11	9	6	4	20810	10988	3198	261	26034	14552	5621	1530
Site-1	1.20	1.60	2.67	9.2	1.20	1.53	2.33	3.6	27	22	17	3	30	24	19	13	6	4	2	2	7	5	3	3	17111	8846	2236	100	22063	12596	4266	925
Site-2	1.60	2.10	3.73	NR	1.53	1.97	3.07	5.5	20	14	10	NR	29	17	11	4	1	1	<1	NR	3	1	<1	<1	12522	6298	1464	NR	16282	9377	3028	440
Site-3	1.67	2.23	4.00	NR	1.60	2.07	3.23	6.0	27	22	15	NR	30	23	18	12	3	2	1	NR	5	3	2	<1	10858	5229	995	NR	14613	8149	2331	372
Site-4	2.43	3.30	6.87	NR	2.27	2.93	4.93	NR	36	25	24	NR	37	30	25	NR	2	1.2	0.7	NR	7	1.6	1.2	NR	6413	2943	359	NR	8784	4762	1130	NR
Site-5	4.83	7.13	NR	NR	4.33	5.73	NR	NR	19	17	NR	NR	24	19	NR	NR	3	1	NR	NR	4.4	2.4	NR	NR	3749	1322	NR	NR	5472	2587	NR	NR

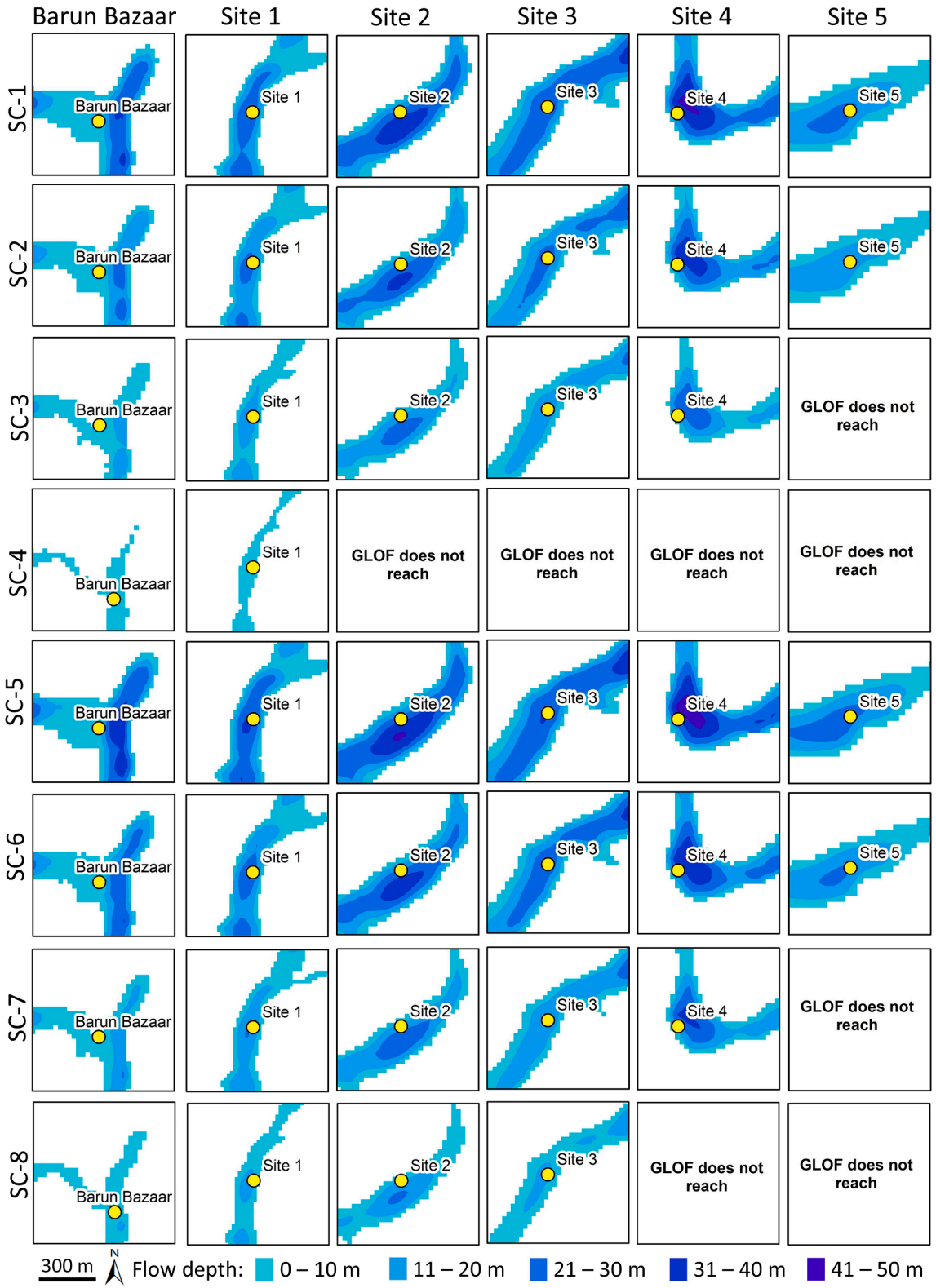

Fig. 10. Scenario-based spatially distributed flow depths (D_f) of Lower Barun GLOFs at different site locations (see Fig. 1 for site locations).

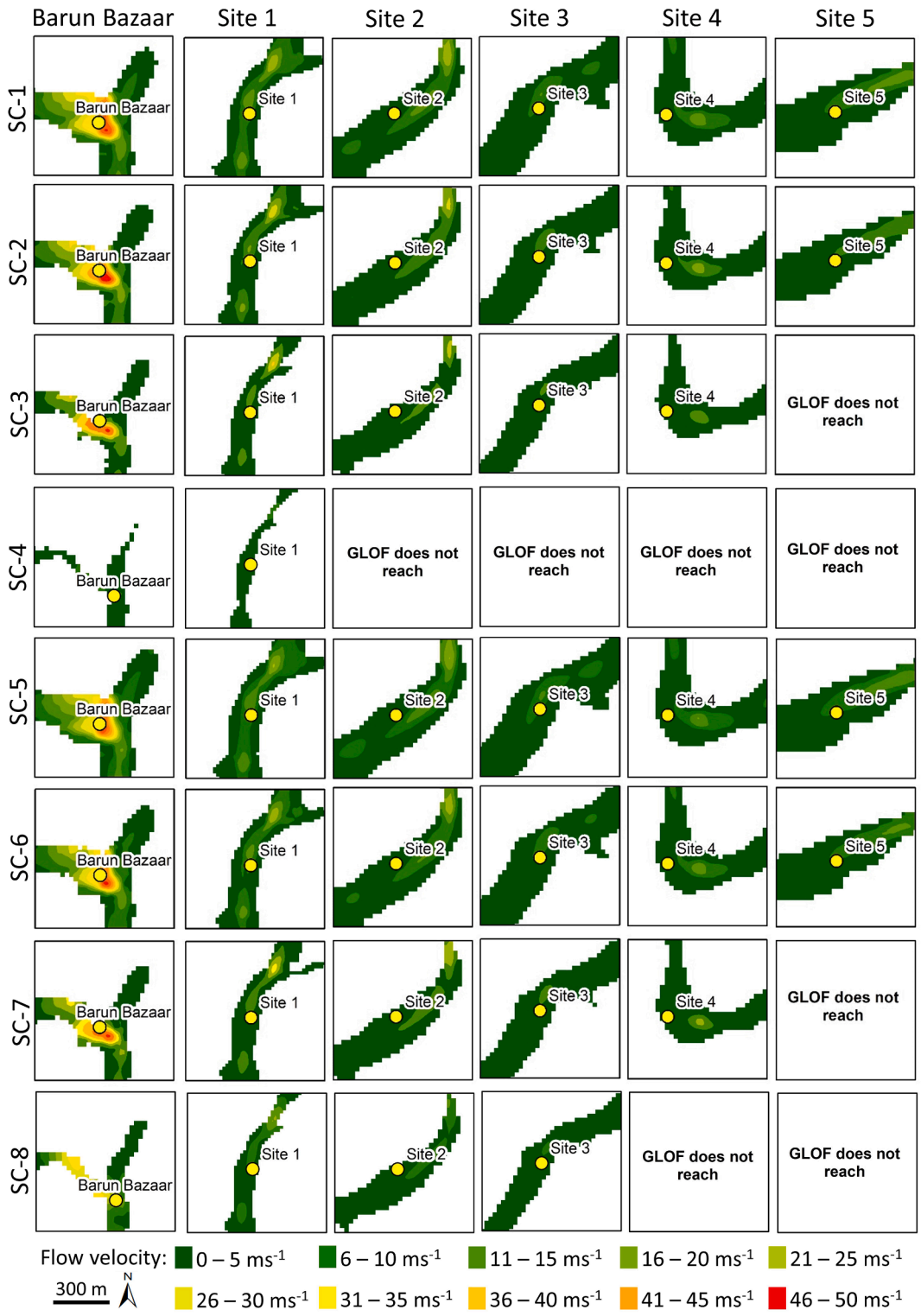

Fig. 11. Scenario-based spatially distributed flow velocities (V_f) of Lower Barun GLOFs at different site locations (see Fig. 1 for site locations).

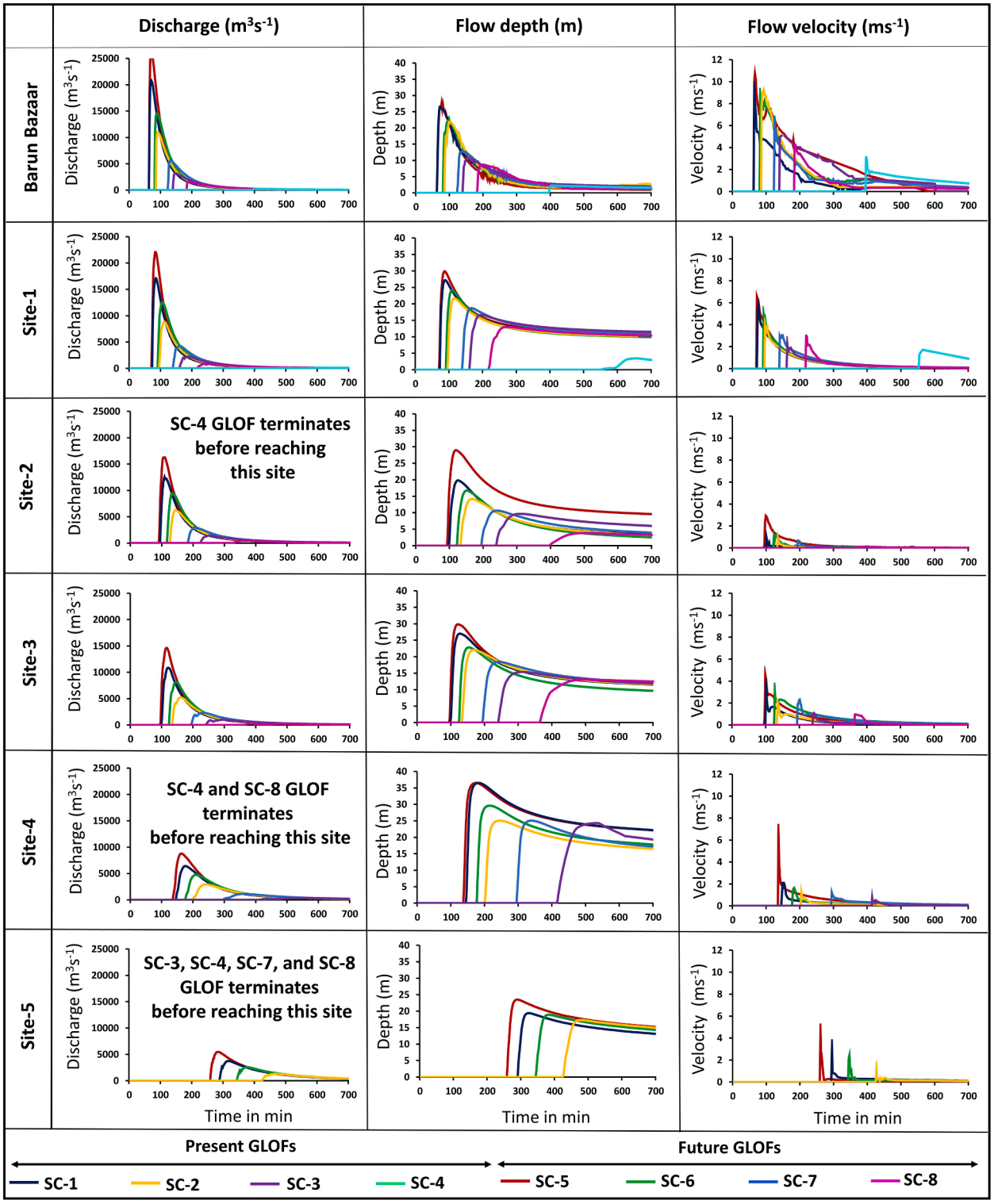

Fig. 12. GLOF scenario-based discharge vs. time, flow depth vs. time, and flow velocity vs. time at each site downstream of Lower Barun Lake.

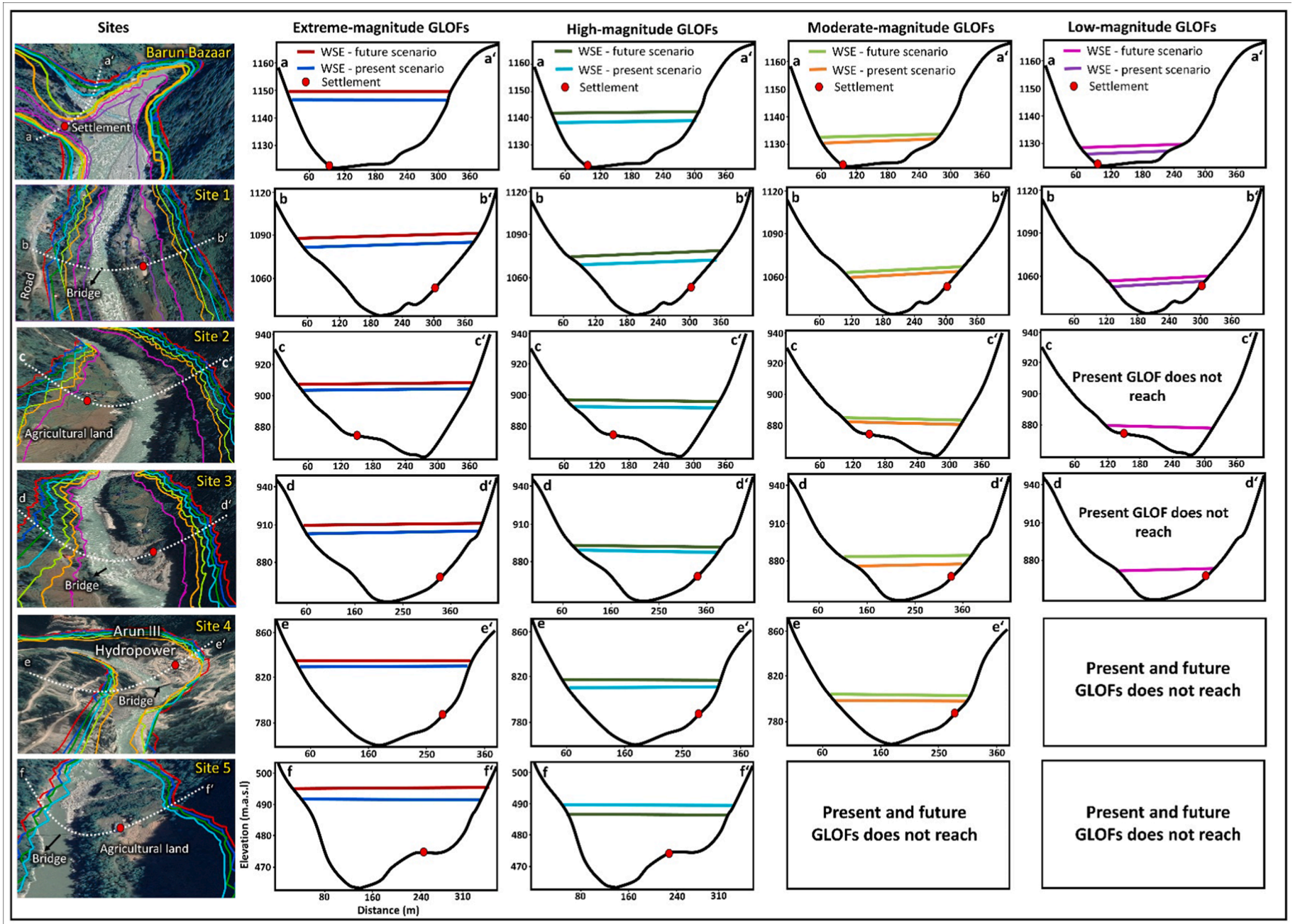

Fig. 13. Google Earth images showing the potential inundation limits in the present and the future GLOFs; cross-sectional profiles across the flow channel at each selected site showing the present and future GLOF-water surface elevation.

magnitude GLOF (Scenario-5) event and indicates a decrease in D_f and V_f by 7 m and 5.4 m s^{-1}, respectively. At Site-5, the flood wave is delayed by 1 h 24 min when compared to Scenario-5. The overall attenuation of Q from Barun Bazaar to Site-5 is 11,965 m^3 s^{-1}.

In the case of a moderate-magnitude future-GLOF (Scenario-7), the arrival of the flood wave to Barun Bazaar is slower by approximately an hour compared to the extreme-magnitude Scenario-5. The flood wave does not reach Site-5 as it loses its flow energy downstream. The at-risk infrastructure upstream of Site-4 remains similar to the above scenarios. At Site-4, V_f reduces to 1.2 m s^{-1} with a discharge of 1130 m^3 s^{-1}. Here, however, D_f rises to 25 m as the flow is obstructed due to the sharp bend in the channel. The I_f decreases by 50% and 33% when compared to Scenario-5 and Scenario-6, respectively.

The hydraulic evaluation of Scenario-8, a low-magnitude GLOF event, reveals a similar GLOF wave to that of Scenario-4, though with a comparable reduction in the peak flood by 592 m^3 s^{-1}. It releases ~9% of the total volume of the lake. The flood attenuates 42 km downstream of the lake before it reaches Site-4. The total I_f along the channel is 6.6 km^2 with mean D_f and V_f values of 6 m and 5.6 m s^{-1}, respectively.

Of the eight GLOF scenarios described above (Section 5.3), only four scenarios, including the potential extreme-magnitude GLOFs (Scenarios-1, and -5), high-magnitude GLOFs (Scenarios-2, and -6) impact all the studied sites (Barun Bazaar, Site-1 to 5) (Figs. 10–13). The moderate-magnitude GLOFs has an impact up to Site-4, as it loses momentum further downstream before reaching Site-5. The low magnitude present-lake event impacts only until Site-1, whereas in the future-lake scenario, impacts down to Site-3.

6. Discussion

6.1. Overtopping hazard

Overtopping flows occur when there is a sudden influx of mass into the lake that displaces the water, forming displacement waves (Clague and Evans, 2000; Westoby et al., 2014). At Lower Barun Lake, the potential overtopping waves that resulted due to avalanche impacts are very short-lived (Fig. 8); the hydrographs reached higher peaks draining a small volume of the lake than that of the breach events (Table 1). Based on the downstream flow hydraulics of the overtopping waves originating from the lake, it is seen that the hazard is minimal for downstream sites as the flood waves attenuate 18 km from the lake. The valley is currently devoid of any settlement until Barun Bazaar, located 29.7 km downstream of the lake. However, at Yangle Kharka, flood waves could potentially affect a couple of existing structures, though minimally, since flow depth and flow velocity reach up to only 1.6 m and 1.4 ms^{-1} (Fig. 8). The bathymetry of the lake (deepest in the west and shoaling to the east) and emptying into a funnel-like outlet would promote the role of tsunami ramp-ups, whose energetic waves could be focused down into the area of ponds and the outlet channel, potentially incising the outlet and allowing a greater outflow. Our calculations show that relatively small avalanches can lead to the ovetopping of the lake.

6.2. Plausibility of 'slow GLOF' and 'fast GLOF' scenarios

The field-collected bathymetric data allows realistic and robust modeling of glacial lake outburst flood events in the Himalaya. We modeled eight potential scenarios, though we recognize that GLOFs could occur in several other ways. For example, the GLOF that occurred from Peruvian Lake Palcacocha in 1941 was a 'to the bottom' breach leading to almost 95% lake water released. However, this is uncommon and only associated with specific topographical settings (Emmer, 2017). Not all GLOFs are similar even if they occur from the same lake (Westoby et al., 2014; Rounce et al., 2016). For example, in some circumstances, a large fraction of a large glacial lake's volume could drain out in a matter of hours or days and still not cause extreme damage downstream except to very low-lying infrastructure. We thus define in our discussion, "fast GLOFs" whose proximal hydrographs peak within minutes of initiation of an outburst event, and "slow GLOFs" whose hydrographs peaks hours after an event starts and may take much longer to complete. A "slow GLOF" may be generated when the drainable volume is constrained by smaller breach dimensions or a large but slowly (hours-long) eroding breach. On the contrary, "fast GLOFs" have much higher peak volume discharge and potential flow energy per unit time as larger and fast-formed breach dimensions allow for an enormous and rapid outlet-discharge. Additionally, a GLOF might initiate slowly but then enter a speedier phase as some critical failure occurs. Hence, "fast" and "slow" GLOFs are not immutable. It is a concept that we introduce here to propel focused discussion. So stated, "fast GLOFs" appear to pose a relatively larger threat to downstream settlements and infrastructures, as demonstrated by our modeling.

The rapidity of a moraine dam's breakup depends on the magnitude of the trigger and the initial disturbance that starts a self-accelerating outflow. It also depends on the amount and distribution of buried ice, the shape of the moraine, the hydraulic pressure at the base of the moraine (hence, the depth of impounded water and height of the moraine), and - an important factor that is rarely considered - the slope and roughness of the bedrock beneath the moraine. The Lower Barun moraine dam is high, and the lake is deep, while a shoaling near the moraine could allow large tsunami runups. Ice and large boulders are present in the moraine (Supplementary-1), but how much of these and their internal arrangements are unknown, as is the shape and slope of the bedrock base beneath the moraine. An assessment of the stability (or metastability) of the moraine dam, or a numerical study of the dynamics of a moraine erosional event, would require geophysical knowledge of the moraine's properties. Lacking knowledge of these, we have focused on what is known.

The lake volume from the 2015 field survey was used to model potential GLOFs in the current state. With the accelerating retreat of connected Lower Barun Glacier, the lake area grew by 0.25 km^2 in the last 5 years (2015–2019) (Fig. S4). This implies that the GLOF hazard will likely change as the melting and retreating glacier fills the enlarging moraine-dammed proglacial lake (Clague and Evans, 1994). The seismically active regime of the Nepal Himalaya has witnessed numerous mass movement events like landslides, avalanches, and rockfalls of various magnitudes (Kargel et al., 2016). These primary events (as witnessed and identified in this study) may act as potential GLOF triggers in the region, especially in the case of Lower Barun Lake, which is surrounded by steep slopes with hanging ice masses. The Langmale GLOF in 2017 (Byers et al., 2018) is an example of such an event that occurred near Lower Barun Lake (Fig. 1). In fact, a landslide— maybe a small moraine collapse— placed directly into the outlet channel, potentially raising the lake by several meters over a several day period, could prove to create a hazardous GLOF if that dam breaks up suddenly.

A low-magnitude avalanche event was witnessed and captured during our fieldwork at the lake site in 2015 (Fig. S5), but it did not result in any known unusual discharge event. However, our modeling of relatively higher magnitude avalanches shows that the frontal moraine of Lower Barun Lake is susceptible to overtopping. The GLOF hazard magnitudes due to avalanches and rockfalls may extend across the full range of the potential GLOF scenarios modeled in this study, the smaller ones being more frequent than the larger. The peak discharge from Lower Barun GLOFs at the current state can reach as high as 20,810 m^3 s^{-1} and can increase by 5224 m^3 s^{-1} in the future. Flow depths and velocities reaching up to 29 m and 11 m s^{-1} can present the valley with great risk. Possibly the typical risk would be to downstream populations along the channel.

The breach depths of the moraine in the two low-magnitude events categorized as slow GLOFs account for only 15% of the total moraine height of the lake, thereby restricting the lake release volume and discharge rate. Such flow events pose no severe threat to the Barun Valley as the flow energy is significantly reduced as it propagates downstream and largely attenuates into a steady flow. These events may

be common in the Himalaya, although likely remain unreported as these floods typically have little or no significant impact on human settlements or infrastructure (Veh et al., 2018).

In a dam breach, the opening forms at the top of the embankment barrier, and as the failure continues, it gradually grows. A breach may also develop as a piping failure, including openings or holes that propagate internal erosion within an embankment and grow outwardly until the opening reaches the top of the embankment (Westoby et al., 2015). Regardless if a breach forms due to embankment overtopping or piping, the size of the opening will increase over time as more and more water passes over or through the opening. Once initiated, a GLOF may progress to an extreme-magnitude event (Huggel et al., 2004), such as scenarios 1 and 4 in this study, if the overtopping wave or the ensuing outflow continues to erode the dam progressively. Therefore, the hazard assessment in the case of a potential extreme-magnitude GLOF cannot be neglected.

By contrast, our evaluation of flood wave behavior for extreme-magnitude GLOFs, high-magnitude GLOFs, and moderate-magnitude GLOFs (both present and the future scenarios) ties them to the production of fast-GLOFs; these hazard events have much higher flow energy compared to the slow-GLOFs. This is because the GLOF peak is reached more rapidly during a progressive breaching event with breach depths sometimes propagating down to the base of the frontal moraine (104 m in case of Lower Barun). Moreover, the breach widths (B_w) are also significantly higher (3 to 4 times) than that of the slow GLOFs allowing higher outflow discharge from the lake. The flow velocities (V_f) along the routed channel are comparatively much higher and therefore travel downstream for longer distances, both values an order of magnitude greater when compared to the slow events.

GLOF triggers and breach formation mechanisms remain uncertain in most cases; however, detailed engineering field investigations can reduce them. This is most often very challenging in harsh terrain such as the Himalaya. However, for disaster preparedness and mitigation, hydraulic modeling of these events provides valuable initial insights and motivations for the needed geophysical field studies and engineering work.

In the aforementioned case of Peru's Palcacocha GLOF, the transport and deposition of giant boulders and finer sediment caused thousands of deaths; casualties would likely have been far smaller if the event only involved water. The amount of ingested, transported, and deposited sediment from possible GLOFs from Lower Barun Lake will be tightly connected to the duration of the peak discharge part of the flood emission, the eroded volume of the moraine dam, and the amount of erodible sediments along the channel. Hence, the sediment component is also tied to whether it is a fast or a slow GLOF.

6.3. Shifting Lower Barun hazard in the future

The Barun-Arun valley, geographically located at the base of Mt. Makalu, has been a favorable region for hydropower generation and currently hosts several infrastructure and hydropower plants that are either fully functional, under construction, or planned. These new developments are opening ways for the communities to expand in the valley. In addition to the enormous hydropower potential the valley possesses, it also hosts several glacial lakes in the high altitude glacierized regions, of which Upper Barun and Lower Barun lakes are the prominent ones (Fig. 1), but as the Langmale flood shows, are not the only dangerous lakes. These high altitude lakes and potential GLOFs present enough downstream threat to impact or destroy the at-risk infrastructure; these potential impacts are intensifying both due to increases in the frequency of hazards and vulnerabilities with increased development. Currently, the valley is not equipped with any mitigation measures to counter these threats, and development planning proceeds as though the risk is nil. This study provides the basis for GLOF preparedness based on the present and future anticipated GLOFs in the valley. The modeled GLOFs were compared for flow hydraulics along the flow channel to evaluate the shift in hazard potential from the current state to future state. Of the eight potential GLOF events we have modeled, the slow (low-magnitude) GLOF events (Scenario-4 and Scenario-8) show similar behavior in both present and future states due to their limited breach and drainable flood volumes. However, the extreme-magnitude cases (Scenario-1 and Scenario-5) reveals a change in flow dynamics and GLOF hazards along the Lower Barun valley. An overall rise in the total inundation modeled in a potential future-lake GLOF event (Scenario-5, 6, and 7) is observed when compared to the current scenario (Scenario-1, 2, and 3) (Figs. 10, 11 and 13). The flow hydraulics Q, V_f, and D_f comparison for the present and future scenarios shows that the Q and V_f shift is more profound than D_f (Fig. 12). This can be attributed to the higher flow energy and discharge, which tends to reduce the frictional resistance compared to a relatively lower discharge event. An increase in Q and V_f by 33% and 36%, respectively, are observed in the future extreme-magnitude event compared to a present extreme-magnitude GLOF. Further, the arrival timings of the GLOF wave at the selected sites decrease in a potential future event due to higher PFV, which results in a higher momentum. The attenuation of the flood wave is seen to be prominent more towards the downstream part of the valley after the flood crosses Site-3, where the difference in flood wave arrival timing increases (Fig. S7). This is due to higher channel friction and lower flow volume as the GLOF propagates downstream. This information becomes vital in designing and implementing any adaptation measures along the Barun and Arun rivers' flow path as part of disaster preparedness.

Furthermore, a comparison of the flow hydraulics revealed that the GLOF arrival at the first site of interest (Barun Bazaar) decreases by 4–16 min in the fast GLOFs. This is due to the comparatively more rapid peaking of V_f in future GLOFs, which is governed by the breach parameters and PFV. This difference in GLOF arrival timing is observed more prominently in the downstream part of the valley (after Site-3). This may be attributed to the loss of flow volume and channel resistance as the flood propagates down the valley. The decreased time carries with it a greater challenge for potential GLOF warning systems and evacuation scenarios. In addition, the total I_f along the flow channel increases by ~15% in case of future GLOFs, compared to potential present events. This is due to the rise of D_f, resulting in higher water-surface elevation in potential future GLOFs (Fig. 13). Although the GLOF hazard in both present and future scenarios are very high, a future event coupled with increasing development intensifies the risk that Lower Barun Lake will pose to the low-lying areas downvalley.

6.4. Future directions

We do not model the erosion dynamics of the breach in the moraine dam. Yager et al. (2012) modeled grain transport in steeply sloping mountain channels and emphasized the important hydrodynamic role of large, immobile protruding obstacles—like large boulders— in reducing the transport of smaller mobile grains. In the case of Lower Barun Lake's end moraine dam, there is a ubiquitous presence within a fine-grained matrix of large boulders— many are 1 to 6 m across (Supplementary section-1), and some are several tens of meters. Whereas 1-m boulders are normal bedload material and can be readily transported in mountain streams along with finer particles over time, they could be transported rapidly during high discharge GLOFs. The larger boulders could remain immobile and retard erosional downcutting such that peak GLOF discharge will be limited, or alternatively an incredible outflow may rapidly mobilize the large boulders and prevent them from armoring the channel. A question for Lower Barun Lake is whether there are enough large boulders in the dam to create an armoring lag deposit. In principle, but not modeled here, a large initial outflow could move large boulders and induce runaway erosion and outflow. Future work should link the overtopping and erosion dynamics, including the critical roles of large boulders and the erosional susceptibility of heterogeneously composed moraine dams, to understand the full process chain, which we have not

done currently in this paper. To undertake this work we would need detailed in situ geophysical and sedimentological data on the moraine, more detailed bathymetry of the lakes, and then theoretical modeling (analytical or numerical) to understand the processes and threshold flows under which the moraine could undergo runaway erosion. Also needed is a better knowledge of the geotechnical properties of potentially unstable masses of rock and ice on the mountain slopes, their potential failure mechanisms and mass flow behavior. Overall, an obvious future direction is to include sediment explicitly in the hydraulic modeling because the sediment will affect the flow depth, arrival time at various points, and deposition at downstream locations. It may thus become useful, in the next step of the investigation, to distinguish and model "dirty GLOFs" (debris-rich) and "clean GLOFs" (mainly water) with an emphasis on viscous flows.

7. Conclusions

Detailed hydrodynamic scenario modeling reveals the hazard potential of moraine-dammed Lower Barun Lake, the deepest and one of the largest known glacial lakes in Nepal. The lake has shown substantial area growth from 0.04 km^2 in 1975 to 2.09 km^2 in 2019. The 'present' (2015) volume of the lake was measured as 112.3 $\times$ 10^6 m^3 and the future volume is calculated as 193.5 $\times$ 10^6 m^3. The flow hydraulics of the overtopping waves caused due to impact from potential avalanches show that the Barun valley is minimally impacted as the upstream part of the valley is devoid of infrastructure. In the case of GLOFs, the maximum drainable volumes in an extreme-magnitude flood originating from the lake in the present and future are calculated to be 101.2 $\times$ 10^6 m^3 and 179 $\times$ 10^6 m^3, respectively. Additionally, we evaluated hydrodynamic flow metrics for sites along the river valley for potential GLOFs originating from both present and the estimated future lake volume. The at-risk infrastructure remains similar in the case of present and future "fast GLOFs." However, the impact changes in the future as flow hydraulics (V_f, I_f, and D_f) increases in potential future events. This is due to larger lake volume resulting in rapid breaching and higher outflow peak and total discharge. Numerous small settlements and infrastructure, including agricultural fields and hydroelectric power projects (under construction or planned), are under potential flood risk. The possible impact of "slow GLOFs" in the valley is significantly less than that of fast events. As both the Lower Barun Lake and the Barun valley evolve, the potential threat from this upstream lake increases. The magnitude of 'fast GLOF' events can significantly affect the downstream infrastructure both in the current state and in the future, affecting up to 70 km downstream of the lake. Based on the present study, regular monitoring of Lower Barun Lake is highly recommended. Further, the results presented here can serve as base information for disaster and flood mitigation. Particularly needed are in situ geophysical studies that may provide constraints on the potential for "fast" versus "slow" GLOFs.

CRediT authorship contribution statement

Ashim Sattar: Conceptualization, Methodology, Writing - original draft, Writing - review & editing. **Umesh K. Haritashya:** Conceptualization, Methodology, Data curation, Writing - original draft, Writing - review & editing. **Jeffrey S. Kargel:** Data curation, Writing - review & editing. **Gregory J. Leonard:** Data curation, Writing - review & editing. **Dan H. Shugar:** Writing - review & editing. **Donald V. Chase:** Methodology, Writing - review & editing.

Declaration of Competing Interest

The authors declare that they have no known competing financial interests or personal relationships that could have appeared to influence the work reported in this paper.

Acknowledgments

We thank the associate editor and two anonymous reviewers for their insightful comments. The authors would like to acknowledge USGS, DigitalGlobe, Planet, Google Earth, Alaska Satellite Facility for various remote sensing data used in the study. We acknowledge the US Army Corps of Engineers for HEC-RAS model. We are grateful for the support from various National Aeronautics and Space Administration (NASA) funding programs for the last several years. Specifically, the following NASA grants made this work possible at different stages: HEC-RAS modeling work under High Mountain Asia grant 80NSSC19K0653 (to UKH, JSK, DHS) and Cryosphere grant 80NSSC20K1442 (to UKH and JSK), RAMMS avalanche modeling under Interdisciplinary Research in Earth Science grant 80NSSC18K0432 (to UKH and JSK), Lower Barun field bathymetric data collection in 2015 under NASA-USAID SERVIR grant NNX12AO96G (to UKH, JSK, GJL).

Appendix A. Supplementary data

Supplementary data to this article can be found online at https://doi.org/10.1016/j.jhydrol.2021.126208.

References

Allen, S.K., Rastner, P., Arora, M., Huggel, C., Stoffel, M., 2016. Lake outburst and debris flow disaster at Kedarnath, June 2013: hydrometeorological triggering and topographic predisposition. Landslides 13 (6), 1479–1491.

Anacona, P.I., Mackintosh, A., Norton, K.P., 2015a. Hazardous processes and events from glacier and permafrost areas: lessons from the Chilean and Argentinean Andes. Earth Surf. Proc. Land. 40 (1), 2–21.

Anacona, P.I., Mackintosh, A., Norton, K., 2015b. Reconstruction of a glacial lake outburst flood (GLOF) in the Engaño Valley, Chilean Patagonia: Lessons for GLOF risk management. Sci. Total Environ. 527, 1–11.

Bajracharya, S.R., Mool, P., 2009. Glaciers, glacial lakes and glacial lake outburst floods in the Mount Everest region. Nepal. Ann. Glaciol. 50 (53), 81–86.

Bajracharya, S.R., Shrestha, B.R., 2011. The status of glaciers in the Hindu Kush-Himalayan region. International Centre for Integrated Mountain Development (ICIMOD).

Bartelt, P., Buehler, Y., Christen, M., Deubelbeiss, Y., Salz, M., Schneider, M., and Schumacher, L.: RAMMS: Rapid Mass Movement Simulation: A numerical model for snow avalanches in research and practice. User Manual v1.5 – Avalanche, Swiss Federal Institute for Forest, Snow and Landscape Research WSL, Birmensdorf, 2013.

Bolch, T., Kulkarni, A., Kääb, A., Huggel, C., Paul, F., Cogley, J.G., Frey, H., Kargel, J.S., Fujita, K., Scheel, M., Bajracharya, S., 2012. The state and fate of Himalayan glaciers. Science 336 (6079), 310–314.

Byers, A.C., Rounce, D.R., Shugar, D.H., Lala, J.M., Byers, E.A., Regmi, D., 2018. A rockfall-induced glacial lake outburst flood, Upper Barun Valley, Nepal. Landslides 16 (3), 533–549.

Byers, A.C., Chand, M.B., Lala, J., Shrestha, M., Byers, E.A., Watanabe, T., 2020. Reconstructing the history of glacial lake outburst floods (GLOF) in the Kanchenjunga Conservation Area, East Nepal: an interdisciplinary approach. Sustainability 12 (13), 5407.

Campbell, J.G., Pradesh, H., 2005. Inventory of Glaciers, Glacial Lakes and the Identification of Potential Glacial Lake Outburst Floods (GLOFs) Affected by Global Warming in the Mountains of India, Pakistan and China/Tibet Autonomous Region. International Centre for Integrated Mountain Development, GP O Box, p. 3226.

Carey, M., Huggel, C., Bury, J., Portocarrero, C., Haeberli, W., 2012. An integrated socio-environmental framework for glacier hazard management and climate change adaptation: lessons from Lake 513, Cordillera Blanca. Peru. Climatic Change 112 (3–4), 733–767.

Christen, M., Kowalski, J., Bartelt, P., 2010. RAMMS: Numerical simulation of dense snow avalanches in three-dimensional terrain. Cold Reg. Sci. Technol. 63 (1–2), 1–14.

Clague, J.J., Evans, S.G., 1994. Formation and Failure of Natural Dams in the Canadian Cordillera, 464. Geological Survey of Canada.

Clague, J.J., Evans, S.G., 2000. A review of catastrophic drainage of moraine-dammed lakes in British Columbia. Quaternary Sci. Rev. 19 (17–18), 1763–1783.

Clague, J.J., O'Connor, J.E., 2015. Glacier-related outburst floods. In Snow and ice-related hazards, risks and disasters. Academic Press, pp. 487–519.

Cook, K.L., Andermann, C., Gimbert, F., Adhikari, B.R., Hovius, N., 2018. Glacial lake outburst floods as drivers of fluvial erosion in the Himalaya. Science 362 (6410), 53–57.

Cuellar, A.D., McKinney, D.C., 2017. Decision-making methodology for risk management applied to Imja lake in Nepal. Water 9 (8), 591.

Dahal, P.R., Paudyal, K.R., Rajaure, S., 2018. Geophysical study on moraine dam of Imja Glacial Lake in Eastern Nepal using Electrical Resistivity Tomography Method. J. Nepal Geol. Soc. 55 (1), 15–22.

Dhote, P.R., Aggarwal, S.P., Thakur, P.K., Garg, V., 2019. Flood inundation prediction for extreme flood events: a case study of Tirthan River, North West Himalaya. Himalayan Geol. 40 (2), 128–140.
Emmer, A., Klimeš, J., Mergilid, M., Vilíme, V., Cochachin, A., 2016. 882 lakes of the Cordillera Blanca: An inventory, classification, evolution and assessment of susceptibility to outburst floods. CATENA 147, 269–279.
Emmer, A., 2017. Glacier retreat and glacial lake outburst floods (GLOFs). In Oxford Research Encyclopedia of Natural Hazard Science.
Emmer, A., 2018. GLOFs in the WOS: Bibliometrics, geographies and global trends of research on glacial lake outburst floods (Web of Science, 1979–2016). Nat. Hazards Earth Syst. Sci. 18 (3), 813.
Evers, F., Heller, V., Fuchs, H., Hager, W.H., Boes, R., 2019. Landslide-generated Impulse Waves in Reservoirs: Basics and Computation. VAW-Mitteilungen, 254.
Farinotti, D., Huss, M., Fürst, J.J., Landmann, J., Machguth, H., Maussion, F., Pandit, A., 2019. A consensus estimate for the ice thickness distribution of all glaciers on Earth. Nat. Geosci. 12 (3), 168–173.
Frey, H., Haeberli, W., Linsbauer, A., Huggel, C., Paul, F., 2010. A multi-level strategy for anticipating future glacier lake formation and associated hazard potentials. Nat. Hazards Earth Syst. Sci. 10 (2), 339–352.
Frey, H., Huggel, C., Chisolm, R.E., Baer, P., McArdell, B., Cochachin, A., Portocarrero, C., 2018. Multi-source glacial lake outburst flood hazard assessment and mapping for Huaraz, Cordillera Blanca, Peru. Front. Earth Sci. 6, 210.
Froehlich, D.C., 1995a. Peak outflow from breached embankment dam. J. Water Resour. Plann. Manage. 121 (1), 90–97.
Froehlich, D.C., 1995b. Embankment Dam Breach Parameters Revisited, Water Resources Engineering, Proceedings of the 1995 ASCE Conference on Water Resources Engineering, San Antonio, Texas.
Fujita, K., Sakai, A., Nuimura, T., Yamaguchi, S., Sharma, R.R., 2009. Recent changes in Imja Glacial Lake and its damming moraine in the Nepal Himalaya revealed by in situ surveys and multi-temporal ASTER imagery. Environ. Res. Lett. 4 (4), 045205.
Fujita, K., Sakai, A., Takenaka, S., Nuimura, T., Surazakov, A.B., Sawagaki, T., Yamanokuchi, T., 2013. Potential flood volume of Himalayan glacial lakes. Nat. Hazards Earth Syst. Sci. 13 (7).
Haritashya, U.K., Kargel, J.S., Shugar, D.H., Leonard, G.J., Strattman, K., Watson, C.S., Shean, D., Harrison, S., Mandli, K.T., Regmi, D., 2018. Evolution and controls of large glacial lakes in the Nepal Himalaya. Remote Sensing 10 (5), 798.
Harrison, S., Kargel, J.S., Huggel, C., Reynolds, J., Shugar, D.H., Betts, R.A., Emmer, A., Glasser, N., Haritashya, U.K., Klimeš, J., Reinhardt, L., 2018. Climate change and the global pattern of moraine-dammed glacial lake outburst floods. Cryosphere 12 (4), 1195–1209.
Haeberli, W., Buetler, M., Huggel, C., Friedli, T.L., Schaub, Y., Schleiss, A.J., 2016. New lakes in deglaciating high-mountain regions–opportunities and risks. Clim. Change 139 (2), 201–214.
Haeberli, W., Linsbauer, A., 2013. Brief communication“ Global glacier volumes and sea level-small but systematic effects of ice below the surface of the ocean and of new local lakes on land”. The Cryosphere 7 (3), 817–821.
Hanisch, J., Delisle, G., Pokhrel, A.P., Dixit, A.M., Reynolds, J.M., Grabs, W.E., 1998. The Thulagi glacier lake, Manaslu Himal, Nepal*Hazard assessment of a potential outburst. Proceedings EighthInternational Congress, International Association for Engineering Geology and the Environment, 21}25 September, Vancouver, Canada, pp. 2209–2215.
Hanisch, J., Pokhrel, A.P., Dixit, A.M., Grabs, W.E., Reynolds, J.M., 1999. GLOF mitigation strategies*lessons learnt from studyingthe Thulagi glacier lake. Nepal [abstract]. J. Nepal Geol. Soc. 20, 163.
Heller, V., Hager, W.H., 2010. Impulse product parameter in landslide generated impulse waves. J. Waterw. Port Coastal Ocean Eng. 136 (3), 145–155.
Hubbard, B., Heald, A., Reynolds, J.M., Quincey, D., Richardson, S.D., Luyo, M.Z., Portilla, N.S., Hambrey, M.J., 2005. Impact of a rock avalanche on a moraine-dammed proglacial lake: Laguna Safuna Alta, Cordillera Blanca, Peru. Earth Surface Processes Landf. 30 (10), 1251–1264.
Huggel, C., Haeberli, W., Kääb, A., Bieri, D., Richardson, S., 2004. An assessment procedure for glacial hazards in the Swiss Alps. Can. Geotech. J. 41 (6), 1068–1083.
Kargel, J., Furfaro, R., Kaser, G., Leonard, G., Fink, W., Huggel, C., Kääb, A., Raup, B., Reynolds, J., Wolfe, D., Zapata, M., 2011. In: ASTER Imaging and Analysis of Glacier Hazards, Chapter 15 in Land Remote Sensing and Global Environmental Change: NASA’s Earth Observing System and the Science of Terra and Aqua. Springer, New York, pp. 325–373.
Kargel, J.S., Leonard, G.J., Shugar, D.H., Haritashya, U.K., Bevington, A., Fielding, E.J., Fujita, K., Geertsema, M., Miles, E.S., Steiner, J., Anderson, E., 2016. Geomorphic and geologic controls of geohazards induced by Nepal’s 2015 Gorkha earthquake. Science 351 (6269).
Kattelmann, R., 2003. Glacial lake outburst floods in the Nepal Himalaya: a manageable hazard? Nat. Hazards 28 (1), 145–154.
Khanal, N.R., Mool, P.K., Shrestha, A.B., Rasul, G., Ghimire, P.K., Shrestha, R.B., Joshi, S. P., 2015. A comprehensive approach and methods for glacial lake outburst flood risk assessment, with examples from Nepal and the transboundary area. Int. J. Water Resour. Dev. 31 (2), 219–237.
Khadka, N., Zhang, G., Thakuri, S., 2018. Glacial lakes in the Nepal Himalaya: inventory and decadal dynamics (1977–2017). Remote Sensing 10 (12), 1913.
Kirschbaum, D., Watson, C.S., Rounce, D.R., Shugar, D., Kargel, J.S., Haritashya, U.K., Amatya, P., Shean, D., Anderson, E.R., Jo, M., 2019. The state of remote sensing capabilities of cascading hazards over High Mountain Asia. Front. Earth Sci. 7, 197.
Klimeš, J., Benešová, M., Vilímek, V., Bouška, P., Rapre, A.C., 2014. The reconstruction of a glacial lake outburst flood using HEC-RAS and its significance for future hazard assessments: an example from Lake 513 in the Cordillera Blanca, Peru. Nat. Hazards 71 (3), 1617–1638.
Kropáček, J., Neckel, N., Tyrna, B., Holzer, N., Hovden, A., Gourmelen, N., Schneider, C., Buchroithner, M., Hochschild, V., 2015. Repeated glacial lake outburst flood threatening the oldest Buddhist monastery in north-western Nepal. Nat. Hazards Earth Syst. Sci. 15 (10), 2425–2437.
Kraaijenbrink, P.D.A., Bierkens, M.F.P., Lutz, A.F., Immerzeel, W.W., 2017. Impact of a global temperature rise of 1.5 degrees Celsius on Asia’s glaciers. Nature 549 (7671), 257–260.
Lala, J.M., Rounce, D.R., McKinney, D.C., 2018. Modeling the glacial lake outburst flood process chain in the Nepal Himalaya: reassessing Imja Tsho’s hazard. Hydrol. Earth Syst. Sci. 22 (7), 3721–3737.
Lavell, A., Oppenheimer, M., Diop, C., Hess, J., Lempert, R., Li, J., Muir-Wood, R., Myeong, S., Moser, S., Takeuchi, K., Cardona, O.D., 2012. Climate change: new dimensions in disaster risk, exposure, vulnerability, and resilience. In: Managing the risks of extreme events and disasters to advance climate change adaptation: Special report of the Intergovernmental Panel on Climate Change. Cambridge University Press, pp. 25–64.
Linsbauer, A., Frey, H., Haeberli, W., Machguth, H., Azam, M.F., Allen, S., 2016. Modelling glacier-bed overdeepenings and possible future lakes for the glaciers in the Himalaya—Karakoram region. Ann. Glaciol. 57 (71), 119–130.
Linsbauer, A., Paul, F., Haeberli, W., 2012. Modeling glacier thickness distribution and bed topography over entire mountain ranges with GlabTop: application of a fast and robust approach. J. Geophys. Res. Earth Surf. 117 (F3).
Majeed, U., Rashid, I., Sattar, A., Allen, S., Stoffel, M., Nüsser, M. and Schmidt, S., 2020. Recession of Gya Glacier and the 2014 glacial lake outburst flood in the Trans-Himalayan region of Ladakh, India. The Science of the Total Environment, pp.144008–144008.
Maskey, S., Kayastha, R.B. and Kayastha, R., 2020. Glacial Lakes Outburst Floods (GLOFs) Modelling of Thulagi and Lower Barun Glacial Lakes of Nepalese Himalaya. Progress in Disaster Science, p. 100106.
Meon, G., Schwarz, W., 1993. Estimation of glacier lake outburst flood and its impact on a hydro project in Nepal. Int. Assoc. Hydrol. Sci. 218, 331–340.
Nie, Y., Sheng, Y., Liu, Q., Liu, L., Liu, S., Zhang, Y., Song, C., 2017. A regional-scale assessment of Himalayan glacial lake changes using satellite observations from 1990 to 2015. Remote Sens. Environ. 189, 1–13.
Osti, R., Egashira, S., 2009. Hydrodynamic characteristics of the Tam Pokhari Glacial Lake outburst flood in the Mt. Everest region, Nepal. Hydrol. Proc.: Int. J. 23 (20), 2943–2955.
Pant, S.R., Reynolds, J.M., 1999. Subsurface electrical imaging tech-niques for the investigation of Thulagi Glacier Lake dam [abstract]. J. Nepal Geol. Soc. 20, 80.
Paul, F., Bolch, T., 2019. Glacier Changes Since the Little Ice Age. In: Geomorphology of Proglacial Systems. Springer, Cham, pp. 23–42.
Regmi, D., Kargel, J.S., Leonard, G.J., Haritashya, U.K., Karki, A., Poudyal, S., 2017. Potential GLOF Hazards and Initiatives taken to minimize its Impacts on Downstream Communities and Infrastructures in Nepal Himalaya. AGUFM 2017, C33A–1166.
Quincey, D.J., Richardson, S.D., Luckman, A., Lucas, R.M., Reynolds, J.M., Hambrey, M. J., Glasser, N.F., 2007. Early recognition of glacial lake hazards in the Himalaya using remote sensing datasets. Global Planet. Change 56 (1–2), 137–152.
Reynolds, J.M., Taylor, P.J., 2004. Inventory of Glaciers, Glacial Lakes and Glacial Lake Outburst Floods, Monitoring and Early Warning Systems in the Hindu Kush-Himalaya Region: Nepal.
Richardson, S.D., Reynolds, J.M., 2000. An overview of glacial hazards in the Himalayas. Quat. Int. 65, 31–47.
Roe, G.H., Baker, M.B., Herla, F., 2017. Centennial glacier retreat as categorical evidence of regional climate change. Nat. Geosci. 10 (2), 95–99.
Rounce, D.R., McKinney, D.C., Lala, J.M., Byers, A.C., Watson, C.S., 2016. A new remote hazard and risk assessment framework for glacial lakes in the Nepal Himalaya. Hydrol. Earth Syst. Sci. 20, 3455–3475.
Rounce, D.R., Watson, C.S., McKinney, D.C., 2017. Identification of hazard and risk for glacial lakes in the Nepal Himalaya using satellite imagery from 2000–2015. Remote Sensing 9 (7), 654.
Sattar, A., Goswami, A., Kulkarni, A.V., 2019a. Hydrodynamic moraine-breach modeling and outburst flood routing – a hazard assessment of the South Lhonak lake, Sikkim. Sci. Total Environ. 668, 362–378.
Sattar, A., Goswami, A., Kulkarni, A.V., Das, P., 2019b. Glacier-surface velocity derived ice volume and retreat assessment in the Dhauliganga basin, Central Himalaya – a remote sensing and modeling based approach. Front. Earth Sci. 7, 105.
Sattar, A., Goswami, A., Kulkarni, A.V., 2019c. Application of 1D and 2D hydrodynamic modeling to study glacial lake outburst flood (GLOF) and its impact on a hydropower station in Central Himalaya. Nat. Hazards 97 (2), 535–553.
Sattar, A., Goswami, A., Kulkarni, A., Emmer, A., 2020. Lake evolution, hydrodynamic outburst flood modeling and sensitivity analysis in the Central Himalaya: a case study. Water 12 (1), 237.
Shugar, D.H., Burr, A., Haritashya, U.K., Kargel, J.S., Watson, C.S., Kennedy, M.C., Bevington, A.R., Betts, R.A., Harrison, S., Strattman, K., 2020. Rapid worldwide growth of glacial lakes since 1990. Nat. Clim. Change 1–7.
Shrestha, A.B., Eriksson, M., Mool, P., Ghimire, P., Mishra, B., Khanal, N.R., 2010. Glacial lake outburst flood risk assessment of Sun Koshi basin, Nepal. Geomatics, Nat. Haz. Risk 1 (2), 157–169.
Shukla, A., Garg, P.K., Srivastava, S., 2018. Evolution of glacial and high-altitude lakes in the Sikkim, Eastern Himalaya over the past four decades (1975–2017). Front. Environ. Sci. 6, 81.
Schneider, D., Huggel, C., Cochachin, A., Guillén, S., García, J., 2014. Mapping hazards from glacier lake outburst floods based on modelling of process cascades at Lake 513, Carhuaz, Peru. Adv. Geosci. 35, 145–155.
Singh, V.P., 1996. Dam Breach Modelling Technology vol. 17, 242.

Somos-Valenzuela, M.A., McKinney, D.C., Byers, A.C., Rounce, D.R., Portocarrero, C., Lamsal, D., 2015. Assessing downstream flood impacts due to a potential GLOF from Imja Tsho in Nepal. Hydrol. Earth Syst. Sci. 19 (3).

Somos-Valenzuela, M.A., Chisolm, R.E., Rivas, D.S., Portocarrero, C., McKinney, D.C., 2016. Modeling a glacial lake outburst flood process chain: the case of Lake Palcacocha and Huaraz, Peru. Hydrol. Earth Syst. Sci. 20 (6), 2519.

Thakur, P.K., Aggarwal, S., Aggarwal, S.P., Jain, S.K., 2016. One-dimensional hydrodynamic modeling of GLOF and impact on hydropower projects in Dhauliganga River using remote sensing and GIS applications. Nat. Hazards 83 (2), 1057–1075.

Uddin, K., Shrestha, H.L., Murthy, M.S.R., Bajracharya, B., Shrestha, B., Gilani, H., Pradhan, S., Dangol, B., 2015. Development of 2010 national land cover database for the Nepal. J. Environ. Manage. 148, 82–90.

USAID, 2014. Affirmative investigations for hydropower projects in Nepal: upper Marsyandi 2, upper Trisuli 1, and Upper Arun. U.S. Agency for International Development's Bureau forEconomic Growth. Education and Environment (USAID/E3), Washington DC.

UNDP – United Nations Development Programme: Community Based Glacier Lake Outburst and Flood Risk Reduction in Nepal, Project Document, UNDP Environmental Finance Services, Kathmandu, Nepal, 2013.

Veh, G., Korup, O., Roessner, S., Walz, A., 2018. Detecting Himalayan glacial lake outburst floods from Landsat time series. Remote Sens. Environ. 207, 84–97.

Veh, G., Korup, O., Walz, A., 2020. Hazard from Himalayan glacier lake outburst floods. Proc. Natl. Acad. Sci. 117 (2), 907–912.

Vilímek, V., Klimeš, J., Emmer, A., Benešová, M., 2015. Geomorphologic impacts of the glacial lake outburst flood from Lake No. 513 (Peru). Environ. Earth Sci. 73 (9), 5233–5244.

Vuichard, D., Zimmermann, M., 1987. The 1985 catastrophic drainage of a moraine-dammed lake, Khumbu Himal, Nepal: cause and consequences. Mt. Res. Dev. 91–110.

Wahl, T.L., 2004. Uncertainty of predictions of embankment dam breach parameters. J. Hydraul. Eng. 130 (5), 389–397.

Wang, W., Gao, Y., Anacona, P.I., Lei, Y., Xiang, Y., Zhang, G., Li, S., Lu, A., 2018. Integrated hazard assessment of Cirenmaco glacial lake in Zhangzangbo valley, Central Himalayas. Geomorphology 306, 292–305.

Watanbe, T., Rothacher, D., 1996. The 1994 Lugge Tsho glacial lake outburst flood, Bhutan Himalaya. Mt. Res. Dev. 16 (1), 77–81.

Westoby, M.J., Glasser, N.F., Brasington, J., Hambrey, M.J., Quincey, D.J., Reynolds, J. M., 2014. Modelling outburst floods from moraine-dammed glacial lakes. Earth Sci. Rev. 134, 137–159.

Westoby, M., Brasington, J., Glasser, N., Hambrey, M., Reynolds, J., Hassan, M., Lowe, A., 2015. Numerical modelling of glacial lake outburst floods using physically based dam-breach models. Earth Surf. Dyn. 3 (1), 171–199.

Worni, R., Huggel, C., Stoffel, M., 2013. Glacial lakes in the Indian Himalayas—From an area-wide glacial lake inventory to on-site and modeling based risk assessment of critical glacial lakes. Sci. Total Environ. 468, S71–S84.

Worni, R., Huggel, C., Clague, J.J., Schaub, Y., Stoffel, M., 2014. Coupling glacial lake impact, dam breach, and flood processes: a modeling perspective. Geomorphology 224, 161–176.

Yager, E.M., Turowski, J.M., Rickenmann, D., McArdell, B.W., 2012. Sediment supply, grain protrusion, and bedload transport in mountain streams. Geophys. Res. Lett. 39, L10402. https://doi.org/10.1029/2012GL051654.

Yamada, T., Sharma, C.K., 1993. Glacier lakes and outburst floods in the Nepal Himalaya. Int. Assoc. Hydrol. Sci. 218, 319–330.